

Review

Li-Rich Mn-Based Cathode Materials for Li-Ion Batteries: Progress and Perspective

Weibin Guo ^{1,2}, Zhangzhao Weng ¹, Chongyang Zhou ¹, Min Han ^{1,*} , Naien Shi ¹, Qingshui Xie ^{2,*} and Dong-Liang Peng ^{2,*}

¹ Strait Institute of Flexible Electronics (SIFE, Future Technologies), Fujian Normal University and Strait Laboratory of Flexible Electronics (SLoFE), Fuzhou 350117, China; ifewbguo@sina.cn (W.G.); ifezzw@fjnu.edu.cn (Z.W.); cyzhou@fjnu.edu.cn (C.Z.); ifeneshi@fjnu.edu.cn (N.S.)

² State Key Laboratory of Physical Chemistry of Solid Surface, Fujian Key Laboratory of Surface and Interface Engineering for High Performance Materials, College of Materials, Xiamen University, Xiamen 361005, China

* Correspondence: ifemhan@fjnu.edu.cn (M.H.); xieqsh@xmu.edu.cn (Q.X.); dlpeng@xmu.edu.cn (D.-L.P.)

Abstract: The development of cathode materials with high specific capacity is the key to obtaining high-performance lithium-ion batteries, which are crucial for the efficient utilization of clean energy and the realization of carbon neutralization goals. Li-rich Mn-based cathode materials (LRM) exhibit high specific capacity because of both cationic and anionic redox activity and are expected to be developed and applied as cathode materials for a new generation of high-energy density lithium-ion batteries. Nevertheless, the difficulty of regulating anionic redox reactions poses significant challenges to LRM, such as low initial Coulombic efficiency, poor rate capability, and fast cycling capacity and voltage decay. To address the existing challenges of LRM, this review introduces their basic physicochemical characteristics in detail, analyzes the original causes of these challenges, focuses on the recent progress of the modification strategies, and then especially discusses the development prospects of LRM from different aspects.

Keywords: Li-rich Mn-based cathode materials; anionic redox activity; modification strategy; lithium-ion batteries



Citation: Guo, W.; Weng, Z.; Zhou, C.; Han, M.; Shi, N.; Xie, Q.; Peng, D.-L. Li-Rich Mn-Based Cathode Materials for Li-Ion Batteries: Progress and Perspective. *Inorganics* **2024**, *12*, 8. <https://doi.org/10.3390/inorganics12010008>

Academic Editor: Torben R. Jensen

Received: 25 October 2023

Revised: 17 December 2023

Accepted: 20 December 2023

Published: 24 December 2023



Copyright: © 2023 by the authors. Licensee MDPI, Basel, Switzerland. This article is an open access article distributed under the terms and conditions of the Creative Commons Attribution (CC BY) license (<https://creativecommons.org/licenses/by/4.0/>).

1. Introduction

The realization of the goal of carbon neutralization is inseparable from the large-scale application of clean energy, which is mostly converted into electricity for use, and it is urgent to develop advanced energy storage devices to efficiently store and utilize clean energy [1–3]. Lithium-ion batteries are efficient energy storage devices that have been widely used in large-scale energy industry, transportation, and consumer electronic devices [4]. However, due to the limited progress in the research of cathode materials, the electrochemical performance of lithium-ion batteries is enhanced slowly [5]. Currently, the main commercialized cathode materials for lithium-ion batteries are olivine-type phosphate systems, spinel-type oxide systems, and layered oxide systems; examples include LiFePO₄ [6–11], LiMn₂O₄ [12–19], LiCoO₂ [20–27], LiMnO₂ [28–36], and LiNi_{0.8}Co_{0.1}Mn_{0.1}O₂ [37,38]. These cathode materials possess unique advantages, but they also have a common disadvantage; that is, relying on cationic redox reactions to contribute to a specific capacity means that the overall specific capacity is not high enough. Thus, there is a pressing need to develop high-specific capacity cathode materials for advanced lithium-ion batteries [39].

Li-rich Mn-based cathode materials (LRM, xLi₂MnO₃·(1-x)LiMO₂, 0 < x < 1, M = Mn, Co, Ni, etc.), which exhibit high specific capacity due to additional anionic redox activity and have been extensively studied, are regarded as promising commercialized cathode materials [40–43]. However, the anionic redox reaction activated by high charging voltage can lead to excessive lattice oxygen oxidation and irreversible release, followed by the

promotion of the migration and dissolution of transition metals, and finally, resulting in the decay of the phase structure [44–46]. Meanwhile, released oxygen can undergo violent interfacial side reactions with the electrolyte, consuming active lithium ions and further hindering lithium-ion diffusion while activating low-voltage redox couples [47–52]. These behaviors contribute to reduced initial Coulombic efficiency, weakened rate performance, and accelerated decay of cycling capacity and voltage [53–55]. To address these challenges and chart future advancements in LRM, it is essential to thoroughly understand their physical and chemical properties and identify potential solutions.

In this review, the history of development, the contradiction of crystal structure, and the diversity of reaction mechanisms of LRM are first introduced comprehensively. Then, the original causes of existing challenges of LRM are analyzed in detail, and the principle and recent progress of modification strategies developed to address these existing challenges are emphatically described. After that, the future development of LRM is prospected from the material level, modification strategy level, and full lifecycle level. This work helps to deepen the understanding of LRM and promote their large-scale commercial application.

2. Development History of LRM

The development of LRM can be traced back to the study of lithium manganese oxide by Johnston and Heikes in 1956. They synthesized the $\text{Li}_x\text{Mn}_{1-x}\text{O}$ system and studied its composition, structure, and magnetic properties [56]. After that, lithium manganese oxide was used as a cathode material for lithium-ion batteries due to its advantages, such as reversible lithium-ion extraction and insertion, environmental friendliness, and low cost [57–59]. However, spinel-structured lithium manganese oxides (such as LiMn_2O_4) do not possess a specific capacity advantage over commercial LiCoO_2 cathode materials [57,60,61]. Although layered lithium manganese oxides (such as LiMnO_2 [28,62] and Li_2MnO_3 [59,63]) have potential specific capacity advantages, their electrochemical stability is poor due to factors such as Mn migration and phase transition [64]. To enhance the electrochemical stability of layered lithium manganese oxides, researchers attempted to introduce other elements to replace part of Mn ions, forming stable layered LiMO_2 compounds. These substitution methods include single-element substitution (such as Al [65], Cr [66], Co [67,68], and Ni [69]) and multi-element substitution (such as Co and Ni [70]). Furthermore, the layered Li_2MnO_3 compound was integrated with the LiMO_2 compound [70]. As a result, the prepared LRM showed enhanced electrochemical stability and ultra-high specific capacity output over a wide range of charge and discharge voltages [71].

3. Crystal Structure of LRM

The crystal structure of LRM is challenging to identify due to the similarity and complexity of the crystal structures of LiMO_2 (space group R-3m) and Li_2MnO_3 (space group C2/m) [72–75]. As shown in Figure 1, researchers have established single-phase solid solution and multi-phase composite models, respectively, for the existence of LiMO_2 and Li_2MnO_3 phases in the form of layered single-phase solid solution [76–79] or multi-phase composite [61,80]. The main dispute between these models concerns the distribution of M atoms in the transition metal layer. Some researchers believe that M atoms are uniformly mixed in the transition metal site; the chemical formula can be written as $\text{Li}_{1+x}\text{M}_{1-x}\text{O}_2$ ($0 < x < 1$). They base this on the linear relationship between the lattice constant of LRM and the proportion of LiMO_2 and Li_2MnO_3 components, which follows Vegard's law of solid solutions [81]. This is supported by transmission electron microscopy and electron diffraction results revealing single-phase solid solution type LRM with either C2/m [82] or R-3m space group [83,84]. Additionally, some researchers believe that there are separation and local clusters of M atoms in the transition metal layer, and the chemical formula can be written as $x\text{Li}_2\text{MnO}_3 \cdot (1-x)\text{LiMO}_2$ ($0 < x < 1$), as evidenced by transmission electron microscopy and electron diffraction results that reveal the existence of multi phases and their heterointerfaces in LRM [85–87]. Although both models are supported by experimental

evidence, the controversy persists because X-ray diffraction and electron diffraction results can be affected by stacking fault [88,89], preventing accurate determination of fine crystal structure information [82,90]. Moreover, transmission electron microscopy results are usually obtained only from the local lattice region. Therefore, to determine the crystal structure of LRM, further advanced characterization methods paired with computational simulations are still needed to comprehensively highlight the advantages of various methods and verify the reliability of evidence from all perspectives [74].

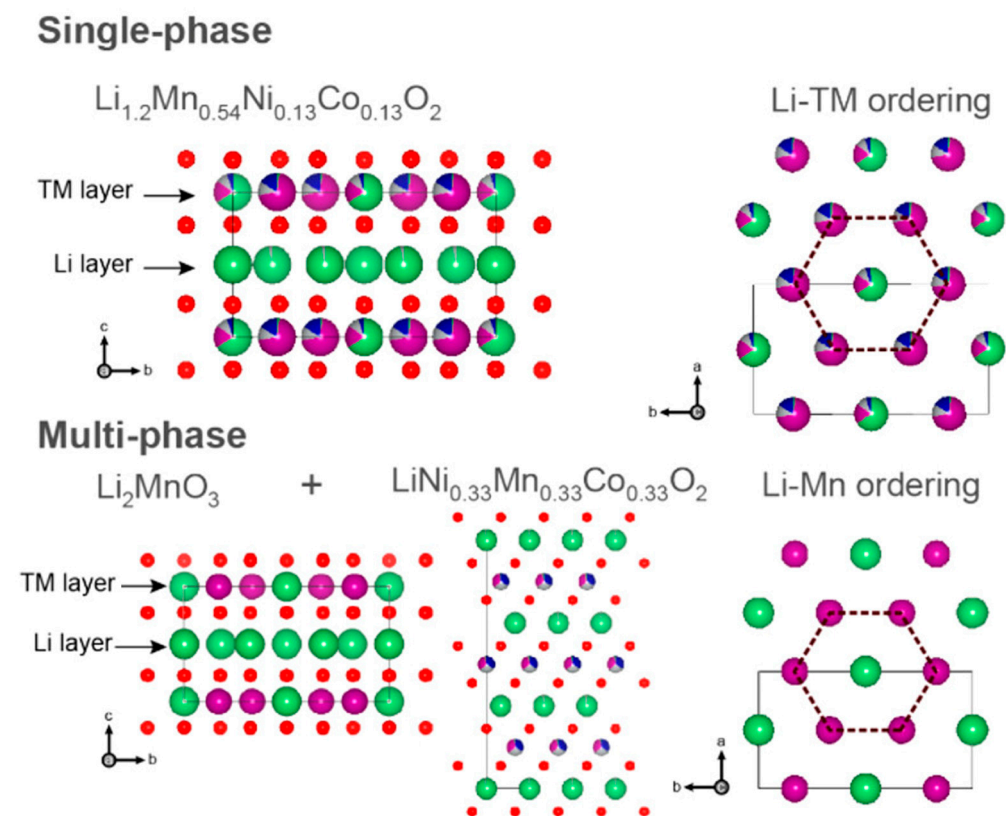


Figure 1. Crystal structure models of LRM. Reproduced with permission from Ref. [75]. Copyright 2021 American Chemical Society.

4. Reaction Mechanism of LRM

The reaction mechanism of LRM involves changes in charge and discharge curves, the origin of high specific capacity, and crystal structure evolution. The change in charge and discharge curves is mainly reflected in the difference between the charge and discharge curves at the initial and second cycles, as shown in Figure 2a,b [80,91]. During the initial charging from point 1 to point 2, lithium ions are removed from the LiMO_2 phase. With the increase in the charging voltage, there is a voltage plateau in the voltage range from point 2 to point 3, owing to lithium-ion extraction and oxygen release in the Li_2MnO_3 phase. During the initial discharging process, lithium ions continue to embed into the LRM over the voltage range from point 3 to point 4. Compared to the initial cycles, although the voltage plateau in the charge curve of the second cycle is no longer present, the voltage hysteresis between the charge and discharge curves reduces.

LRM exhibits a significantly higher specific capacity compared to what is contributed by cationic redox reactions. The additional specific capacity is typically attributed to anionic redox reactions. Partial lattice oxygen can contribute to specific capacity through the reversible conversion of O^{2-} and O_2^{2-} states during the charging and discharging process of LRM [92]. Regarding the source of partial lattice oxygen activity, compared with conventional Li-M oxides, lithium-rich Li-M oxides feature an oxygen atomic coordination structure consisting of two Li-O-M and one Li-O-Li configuration [93]. In the Li-O-M

configuration, O 2p orbitals form hybridized molecular orbitals with the transition metal. However, due to the large energy difference between O 2p and Li 2s orbitals in the Li-O-Li configuration, hybridized molecular orbitals between O 2p and Li 2s orbitals cannot form. The energy level of such a Li-O-Li state is intermediate between the hybridized O bonding states and the anti-bonding transition metal states. When the charging voltage is raised to the high voltage segment, O 2p orbitals in the Li-O-Li configuration preferentially release electrons, stimulating oxygen redox reactions for charge compensation [74,93].

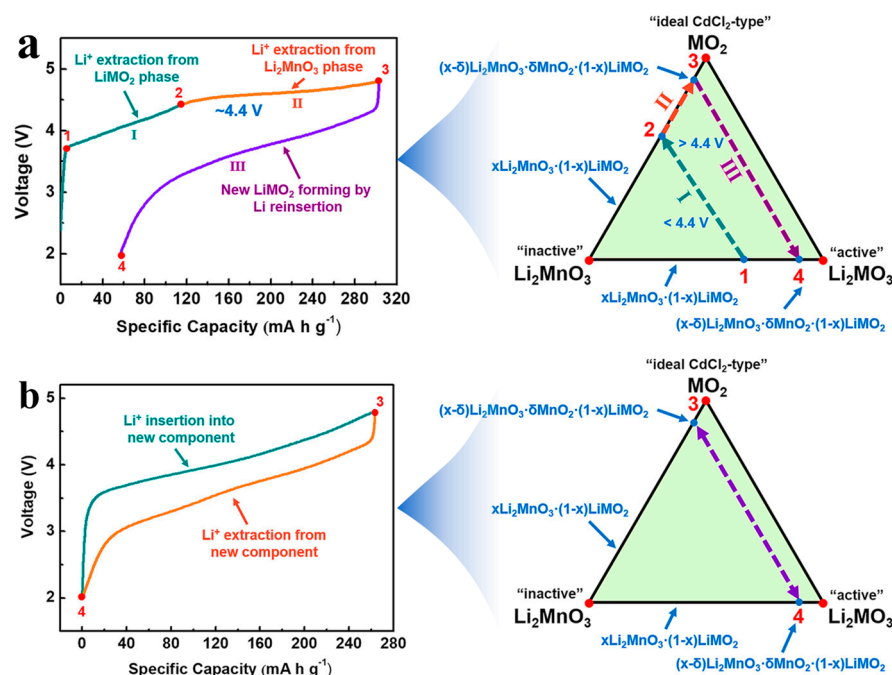


Figure 2. Charge and discharge curves of LRM and the corresponding reaction pathway phase diagram in the (a) initial and (b) second cycles. Reproduced with permission from Ref. [91]. Copyright 2021 Wiley.

The crystal structure evolution process in LRM involves the gradual loss of lithium ions from the transition metal layer of the Li_2MnO_3 phase due to repeated lithium-ion removal and insertion during cycling. This leads to an irreversible transformation of the Li_2MnO_3 phase into a LiMO_2 phase [94]. Moreover, nickel ions migrate from the bulk lattice to the surface lattice during cycling, thus forming a nickel-deficient bulk region and a nickel-rich surface reconstruction layer [95]. Furthermore, along with internal phase transformation and transition metal ion migration, lattice breakdown, vacancy condensation, micro-cracks, and pore accumulation will gradually occur in the bulk phase. These changes cause lattice distortion and amorphous conversion of internal grains in the bulk, gradually leading to the formation of spinel phases with different orientations [94,96].

5. Key Challenges of LRM

LRM exhibits high specific capacity due to the additional anionic redox activity. However, anionic redox reactions activated at high charging voltage can cause a series of problems (Figure 3), including irreversible oxygen release, surface/interface structural phase transitions, transition metal dissolution, and interfacial side reactions. These issues will destroy the crystal structure, block the lithium-ion diffusion pathway, and hinder charge transfer, thereby reducing the initial Coulombic efficiency (ICE), deteriorating the rate performance, and exacerbating the fading of capacity and voltage, which greatly limits the large-scale commercial viability of LRM [97–99].

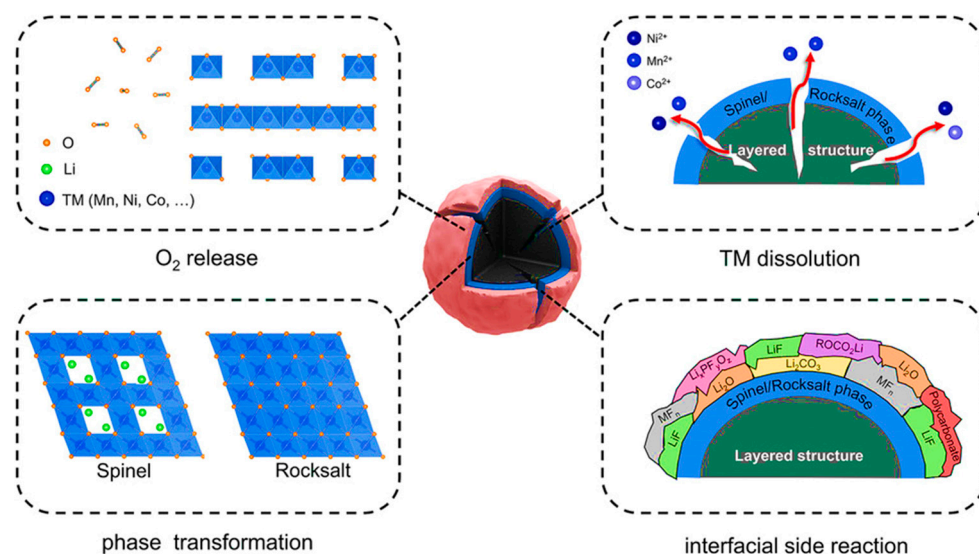


Figure 3. Diagram of the surface structure decay of LRM. Reproduced with permission from Ref. [99]. Copyright 2022 Wiley.

A low ICE is numerically represented by an initial charging-specific capacity that is significantly higher than the initial discharging capacity. The reason is that the voltage plateau at a charging voltage exceeding 4.4 V in the LRM's charging curve contributes significantly to the initial specific charging capacity, but this voltage plateau is irreversible during the initial discharge cycle [100,101]. The disappearance of the voltage plateau in the initial discharge curve means that a large number of lithium-ions removed from the LRM during the initial charging process are not embedded back into the LRM during the subsequent discharging process. Lithium-ion failure to reinsert into the LRM may result from lattice oxygen release, crystal structure phase transitions, transition metal ion migrations, and blockages or collapses of lithium-ion return paths to their original points [102–104].

The rate performance of LRM is primarily limited by lithium-ion diffusion rates within the material and charge transfer rates at the electrode/electrolyte interface [105,106]. Among them, several factors contribute to limiting lithium-ion diffusion in LRM, which can be divided into three main categories. Firstly, during the charging process, lithium-ion in the transition layer of the Li_2MnO_3 phase must migrate to the lithium layer via stabilized tetrahedral sites, and the overall migration path is longer and the repulsion effect is relatively larger during the migration process compared to that of lithium-ion in the LiMO_2 phase [107]. Meanwhile, the Li_2MnO_3 phase and its active MnO_2 components exhibit poor kinetics, and the dynamic barrier of lithium-ion diffusion at the interface between the Li_2MnO_3 component and electrolytes is higher [105]. Secondly, the diffusion path of lithium-ion can only be along the direction parallel to the lithium layer, and the crystal face perpendicular to the lithium layer has no electrochemical activity for the transport of lithium-ion, preventing them from providing a suitable path for lithium-ion transport [108–110]. Thirdly, due to the poor electrical conductivity of the Li_2MnO_3 phase, LRM exhibits low electrical conductivity [105,106,111].

Serious voltage and capacity decay during cycling is mainly due to the release of lattice oxygen, which triggers the conversion of redox couples, defect formation, phase structure transformations, and interfacial side reactions [52,112–116]. During the initial cycle, the capacity is primarily provided by redox couples, such as $\text{Ni}^{2+}/\text{Ni}^{3+}$, $\text{Ni}^{3+}/\text{Ni}^{4+}$, and O^{2-}/O^- , but the release of lattice oxygen will activate lower voltage redox couples, such as $\text{Mn}^{3+}/\text{Mn}^{4+}$ and $\text{Co}^{2+}/\text{Co}^{3+}$, resulting in a continuous decrease in the average valence state of transition metal ions and then accelerate the voltage decay [52]. Meanwhile, a decrease in the Mn element's valence state stimulates the Jahn–Teller effect, which intensifies Mn element dissolution [113,114,117]. Moreover, triggering anionic redox reactions reduces

the formation energy and diffusion barriers of oxygen vacancies, leading to nanohole formation and crystal structure transformations [115,118]. Over time, the layered LRM structure gradually transforms into a spinel and disordered rock-salt phase [113]. In addition, the released lattice oxygen will aggravate the interfacial side reaction and further deteriorate the cycling performance [114].

6. Modification Strategies of LRM

Considering the significant challenges faced by LRM, current modification strategies primarily center on morphology design, phase composition and structure regulation, surface coating, bulk doping, defective structure construction, and binder research.

6.1. Morphology Design

Morphology design primarily involves controlling the initial precursor morphology by adjusting preparation methods and process parameters during the precursor's production. This ultimately leads to obtaining the desired final morphology through subsequent high-temperature sintering [119–123]. LRM exhibits a wide variety of morphologies, such as fusiform porous micro-nano structure [119], double-layer hollow microspheres [120], nanowires [121], irregular particles [122], and three-dimensional cube-maze-like structures [123]. To prepare double-layer LRM hollow microspheres, Ma et al. [120] employed the co-precipitation method to synthesize spherical transition metal hydroxide precursors. They then pre-calcined the precursors to form corresponding transition metal oxides, achieving a hollow structure in the spherical transition metal oxides by controlling the pre-calcination temperature. Mixing the transition metal oxide with lithium hydroxide and calcining at high temperatures resulted in the target morphology (Figure 4a). The synthesized double-layer LRM hollow microspheres enhanced structural stability and optimized lithium-ion diffusion paths and charge transport characteristics, leading to significant rate performance improvement (Figure 4b). Additionally, Liu et al. [123] used the hydrothermal method to prepare a three-dimensional cube-maze-like carbonate precursor by controlling the proportion of solvent components. They combined this approach with solid phase sintering to produce a three-dimensional cube-maze-like LRM with exposed {010} active planes (Figure 4c). The three-dimensional cube-maze-like architecture increases specific surface area and shortens lithium-ion diffusion paths, ultimately enhancing the rate capability and cycling stability of LRM (Figure 4d).

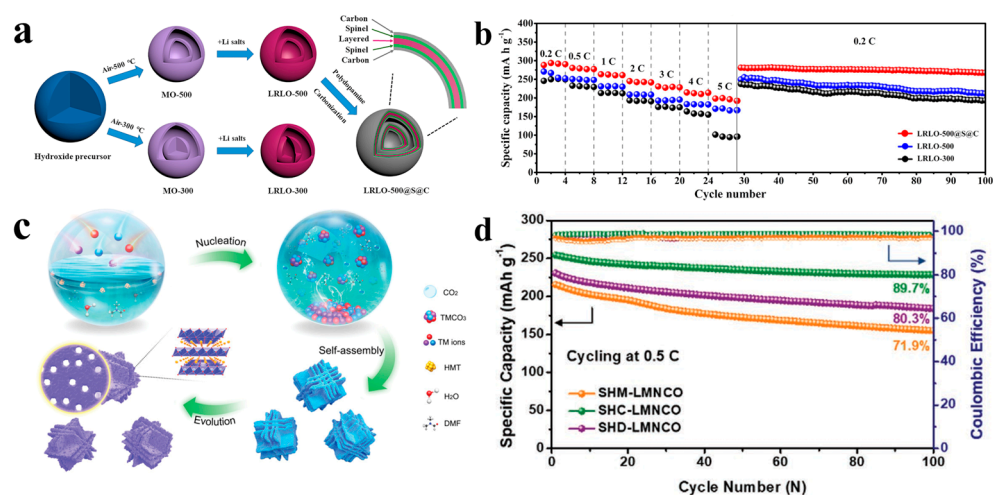


Figure 4. (a) Schematic diagram of the synthesis process of double-layer LRM hollow microspheres. (b) The corresponding rate capability. Reproduced with permission from Ref. [120]. Copyright 2019 Elsevier. (c) Schematic diagram of the preparation process of three-dimensional cube-maze-like LRM. (d) The corresponding cycling performance. Reproduced with permission from Ref. [123]. Copyright 2019 Wiley.

6.2. Phase Composition and Structure Regulation

Phase composition and structure regulation primarily involve adjusting the component distribution and structural frameworks during both precursor and final LRM production [124–132]. Firstly, for phase component regulation, Wu et al. [124] synthesized agglomerated-sphere LRM with a concentration gradient in the phase component using the co-precipitation method. Figure 5a illustrates that Mn element concentration decreases linearly from the particle center to the surface, while Ni and Co element concentrations increase linearly. By combining high-capacity particle center and cycle-stable surface phases, voltage fading is effectively suppressed, and cycling stability is improved (Figure 5b, c). Secondly, for phase structure regulation, transition metal ions can migrate into lithium sites within the lithium layer relatively easily through tetrahedral sites between the transition metal layer and the lithium layer in conventional O3-type LRMs. This irreversible migration leads to structural rearrangement and voltage attenuation [125–128]. Eum et al. [128] used the ion exchange method to prepare O2-type LRM to inhibit this phenomenon. In the O2-type phase structure, face-shared transition metal ions generate strong electrostatic repulsion, preventing their transfer to lithium sites. Additionally, these face-shared sites promote reversible transition metal ion transfer back to the original sites in the transition metal layer during discharge. Finally, co-regulation of phase composition and structure can also be employed. For example, constructing the spinel/layered heterostructure [129–132] with good structural compatibility creates three-dimensional lithium-ion diffusion channels, enhances lattice oxygen stability, and restrains phase transitions and interfacial side reactions. This approach improves the rate and cyclic performance of LRM.

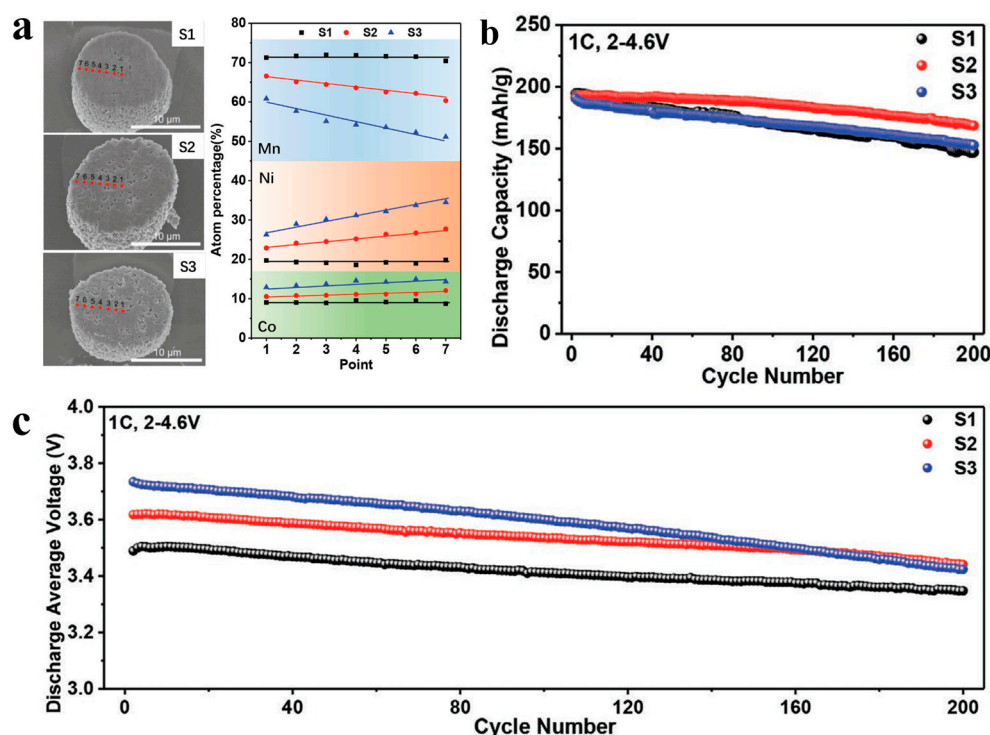


Figure 5. (a) Cross-section SEM images and compositional gradient curves of the agglomerated-sphere LRM with phase component concentration gradient. (b,c) The corresponding (b) capacity and (c) voltage cycling performance. Reproduced with permission from Ref. [124]. Copyright 2021 Wiley.

6.3. Surface Coating

Surface coating primarily serves to protect LRM from direct electrolyte erosion, stabilize surface lattice oxygen, inhibit phase transitions, and reduce interfacial side reactions [133–146]. Surface coating materials can be broadly divided into three categories. The first category is active materials containing lithium, such as Li_2MnO_3 [133],

$\text{Li}_4\text{V}_2\text{Mn}(\text{PO}_4)_4$ [134], and LiFePO_4 [135]. Kim et al. [133] used dip-dry combined with high-temperature calcination to coat Li_2MnO_3 with the same crystal framework as the bulk phase on the surface of LRM, achieving a seamless interface connection that effectively reduces transition metal ion mixing and inhibits phase transitions. The second category consists of non-active materials without lithium, including oxides [136,137], phosphates [138,139], and fluorides [140,141]. Zhang et al. [136] applied atomic layer deposition technology to construct Al_2O_3 and TiO_2 coatings on the surface of LRM. Since the TiO_2 coating appeared as particles on the surface of LRM, while the Al_2O_3 coating showed good uniformity and consistency, materials with the Al_2O_3 coating layer exhibited better cycling stability. The third category comprises functional materials, such as fast ionic conductors [142–144], piezoelectric materials [145], and dielectric materials [136]. Xu et al. [144] used potassium Prussian blue with good ion conduction properties as the coating material for LRM (Figure 6a). The three-dimensional open frame structure of the potassium Prussian blue coating layer provides sufficient interstitial sites and transmission channels for lithium-ion transport, protecting LRM from electrolyte corrosion and inhibiting interfacial side reactions. As a result, the coated sample displays remarkably enhanced rate capability and cycling stability (Figure 6b,c).

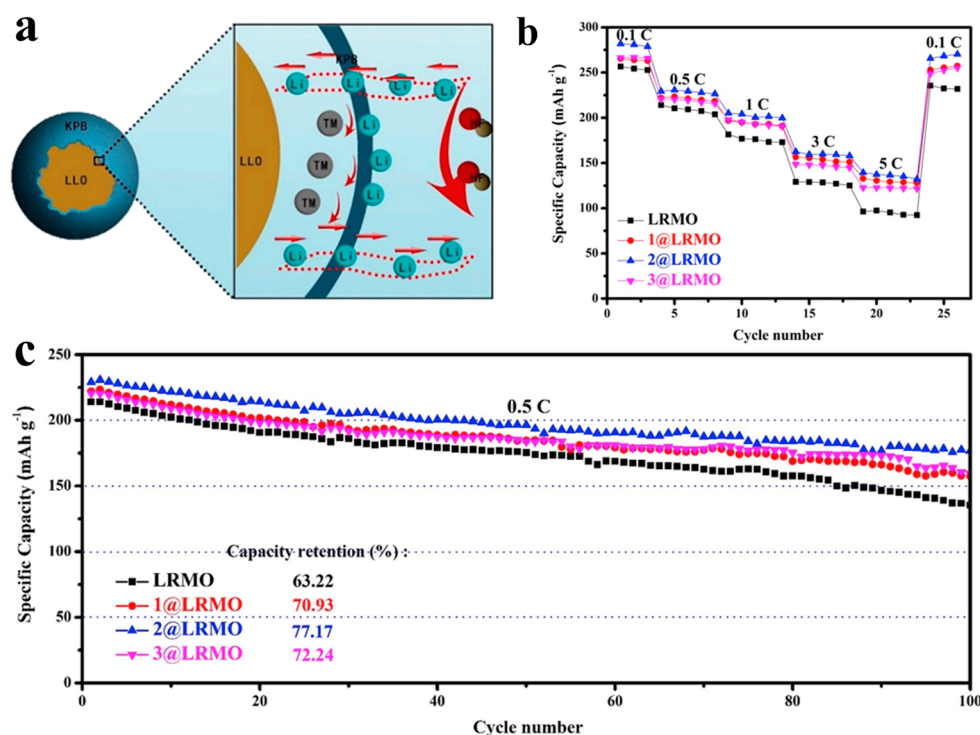


Figure 6. (a) Schematic diagram of the working mechanism of potassium Prussian blue coated LLO. (b,c) The corresponding rate capability (b) and cycling performance (c). Reproduced with permission from Ref. [144]. Copyright 2020 Elsevier.

6.4. Bulk Doping

Bulk doping involves introducing dopants during the precursor's production to enhance lithium-ion transport by expanding diffusion channels, suppressing transition metal ion migration, and stabilizing lattice oxygen through a pinning effect [48,147–166]. Doping can be carried out in single-ion or multi-ion forms, with single-ion doping involving either a single cation or anion. Commonly used single cations include Na^+ [147–149], K^+ [150], Mg^{2+} [151], Al^{3+} [48], Sb^{3+} [152], Nb^{5+} [153] and W^{6+} [154,155]. He et al. [148] introduced Na^+ ions into the co-precipitation process for carbonate precursor synthesis, achieving a uniform distribution of Na^+ in the LRM. The uniform distributed Na^+ effectively inhibited detrimental solid–liquid interface corrosion and transition metal ion migration, enhancing structural and cyclic stability. Single anions commonly employed are F^- [156,157],

S^{2-} [158], and polyanion [159]. Li et al. [159] directly incorporated boracic polyanion to regulate the electronic structure during LRM preparation via the sol-gel method. The lowered M–O bond covalence and decreased top of the O 2p band mitigated changes in the electronic structure of the O 2p band during charging and discharging, improving thermal and cycling stability (Figure 7a–c). In addition, various multi-ions can be used, such as (Na^+ and Si^{4+}) [160], (Al^{3+} and Ti^{4+}) [161], (Ni^{2+} and SO_4^{2-}) [162], (Fe^{3+} and Cl^-) [163], (Nb^{5+} and F^-) [164] and (Na^+ and F^-) [165,166]. Among these, Zheng et al. [166] introduced both Na^+ and F^- ions in the solvothermal preparation process of the precursor (Figure 7d). The additional formation of Na–O and TM–F bonds regulated the local atomic structure and reduced the energy of the TM 3d–O 2p and non-bonding O 2p bands. This led to a reduction in lithium-ion diffusion activation energy and an increase in oxygen vacancy formation energy, simultaneously improving lattice oxygen stability, rate performance, and cycling stability (Figure 7e,f).

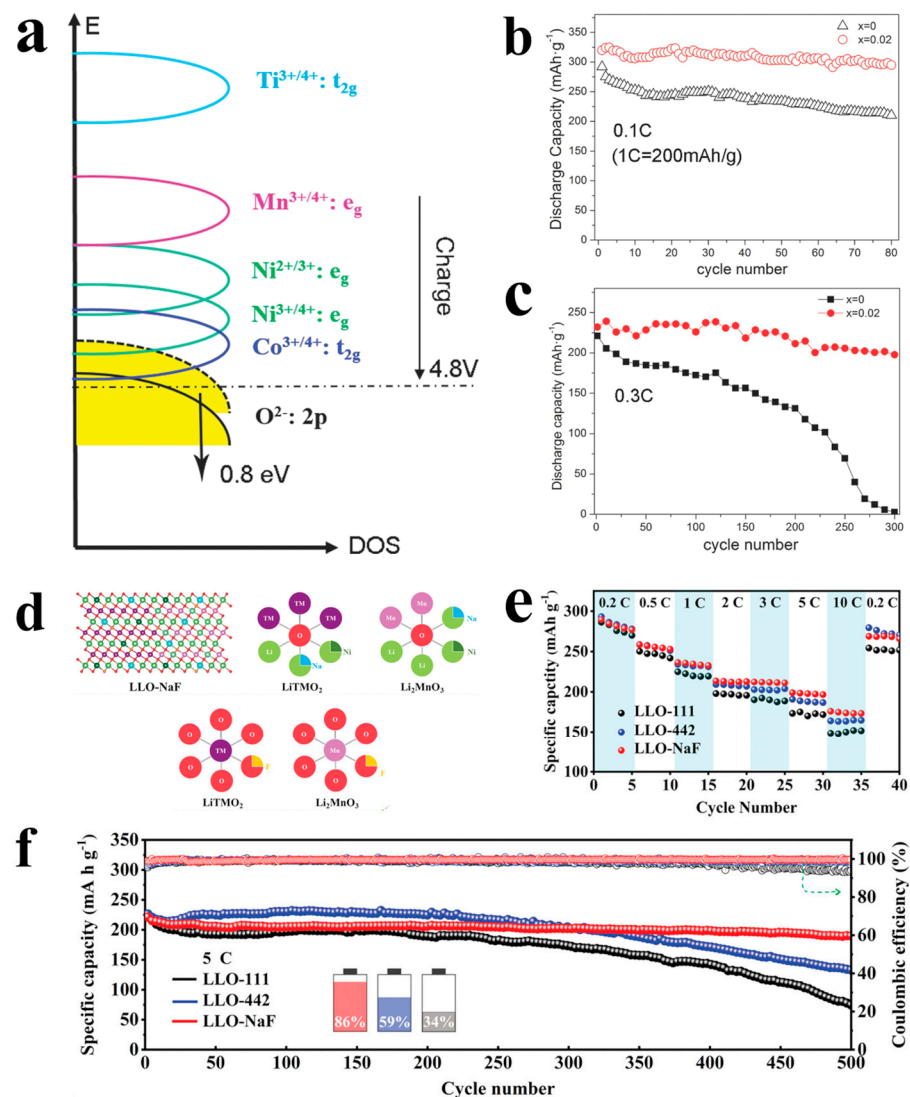


Figure 7. (a) Schematic diagram of charge compensation mechanism of boracic polyanion doped LRM. (b,c) The corresponding cycling performances. Reproduced with permission from Ref. [159]. Copyright 2014 Wiley. (d) Diagram of the local atomic coordination structure of Na^+ and F^- co-doped LRM. (e,f) The corresponding rate capability (e) and cycling performances (f). Reproduced with permission from Ref. [166]. Copyright 2021 Wiley.

6.5. Defective Structure Construction

The construction of the defective structure is achieved by regulating reaction conditions during the addition of a lithium source and subsequent calcination process or surface modification for the final LRM product. The benefits include reducing lithium-ion diffusion energy barriers and improving surface lattice oxygen stability [167–173]. Common defects include cationic vacancies [167,168], anionic vacancies [169–171], and other types of defects [170,172,173]. Cationic vacancies, such as lithium vacancies, were constructed by Liu et al. [167] by controlling the amount of the added lithium source in the calcination process (Figure 8a). This effectively lowered the diffusion energy barrier of lithium ions and improved the utilization rate. Meanwhile, the in situ formation of lithium vacancies induced the development of surface spinel coating and Ni-doping in the lithium layer. The combined strategies resulted in enhanced initial Coulombic efficiency, rate performance, and cycling stability of LRM (Figure 8b–e). For anionic vacancies, such as oxygen vacancy, Qiu et al. [169] used the decomposition of ammonium bicarbonate to perform a gas–solid interface reaction with LRM, creating oxygen vacancies. The presence of oxygen vacancies increased lithium-ion mobility, limited surface gas emissions, and reduced interface impedance, thereby enhancing rate performance. Regarding other types of defects, such as stacking faults, Liu et al. [172] prepared LRM with varying degrees of stacking faults by controlling the type of molten salt and reaction temperature in the molten-salt method. They found that samples with more stacking faults showed higher reversible capacity.

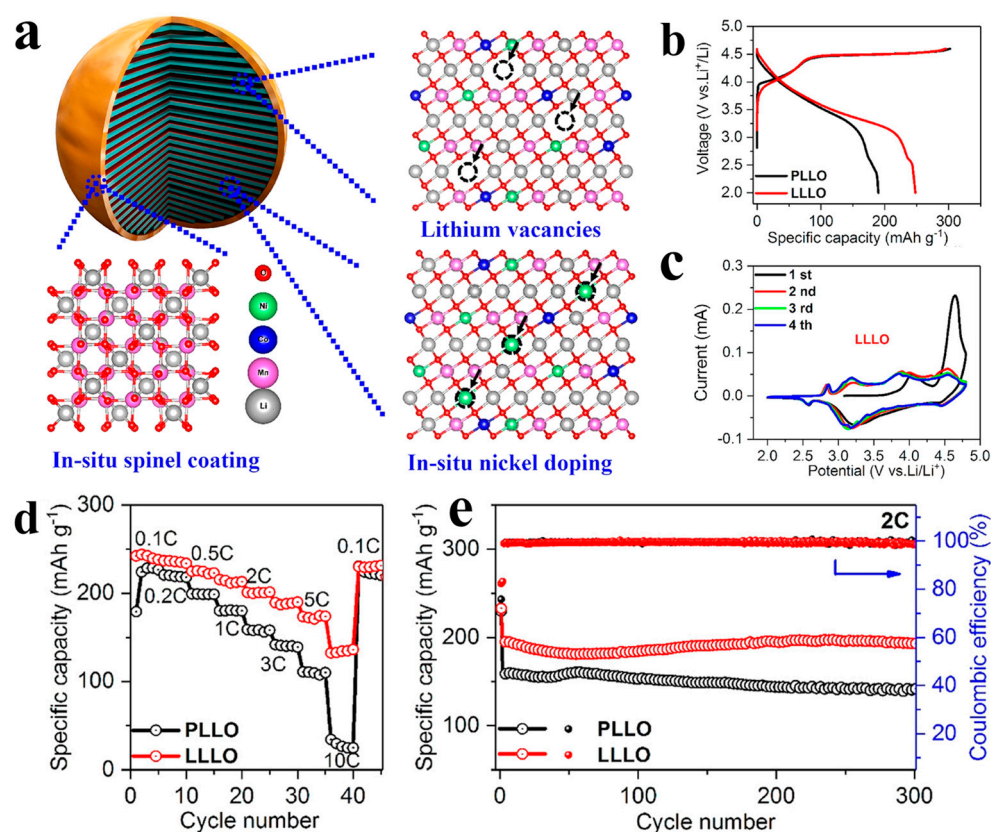


Figure 8. (a) Diagram of the crystal structure of LLLO particle modified by lithium defect engineering. (b–e) The corresponding initial charge and discharge curves (b), cyclic voltammograms (c), rate capability (d), and cycling performance (e). Reproduced with permission from Ref. [167]. Copyright 2019 American Chemical Society.

6.6. Binder Research

The primary purpose of binder research is to inhibit transition metal ion transfer and improve adhesion to LRM. In addition to commonly used polyvinylidene fluoride,

other binders include polyacrylic acid and polyacrylonitrile [174,175]. For example, Yang et al. [174] employed polyacrylic acid as the binder (Figure 9a). This effectively isolated and mitigated electrolyte erosion on LRM. The hydrogen ions in polyacrylic acid can exchange with the lithium ions on the LRM surface, forming a proton-doped surface layer that hinders transition metal ion transfer. This process reduces voltage decay and enhances cycling stability (Figure 9b, c). Additionally, Xu et al. [175] used polyacrylonitrile as a binder (Figure 9d). The carbon–nitrogen triple-bond in polyacrylonitrile can form coordination bonds with unstable transition metal ions on the LRM surface. These bonds increase the migration energy barrier for irreversible transition metal ions transfer. Meanwhile, the coordination bond enhances the adhesion between polyacrylonitrile and LRM, reducing electrolyte erosion and improving adhesion to the aluminum foil current collector. This results in enhanced voltage and cycling stability (Figure 9e, f).

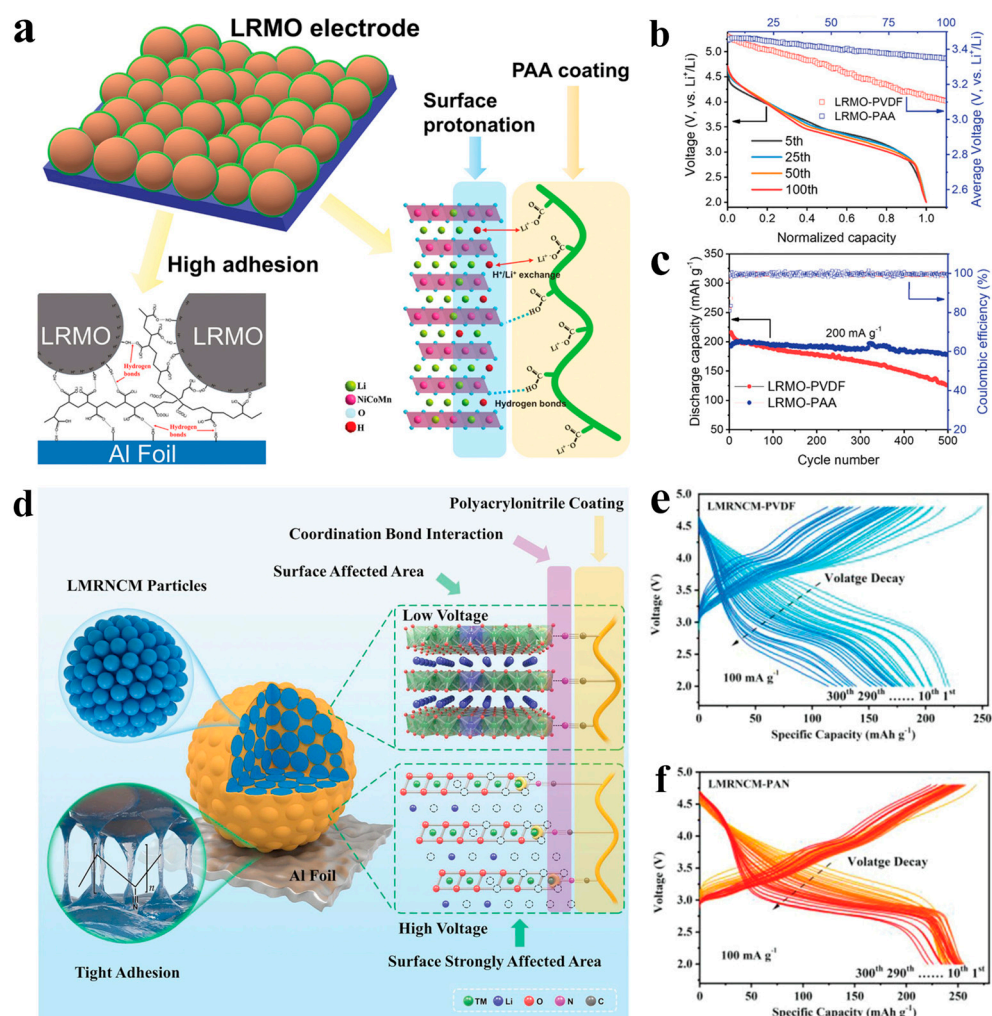


Figure 9. (a) Schematic diagram of the mechanism of polyacrylic acid as the binder. (b,c) The corresponding voltage (b) and capacity (c) cyclic performance. Reproduced with permission from Ref. [174]. Copyright 2020 Wiley. (d) Schematic diagram of the mechanism of polyacrylonitrile as the binder. (e,f) The corresponding cyclic voltage performance. Reproduced with permission from Ref. [175]. Copyright 2022 Wiley.

7. Summary and Prospects

In this review, the development history, synthesis methods, crystal structure, and reaction mechanism of LRM are introduced, and the current key challenges are analyzed. Then, the recent progress of modification strategies to overcome these challenges is described in detail. While these strategies have mitigated problems such as low initial Coulombic

efficiency, poor rate performance, fast cycling capacity and voltage fading to a certain extent, there remain numerous challenges at different levels that need to be considered and solved in future research work for the commercial viability of LRM.

The first challenge is at the material level. Voltage decay and hysteresis are still critical electrochemical performance issues that need to be solved. To solve these problems, it is urgent to deepen the comprehension of the crystal structure and reaction mechanism of LRM. In the future, advanced characterization techniques and computational simulation methods could be used to identify the unresolved crystal structure and clarify the unresolved reaction mechanism at the atomic and energy levels. This would establish a clear structure–activity relationship and further improve the comprehensive electrochemical performance of LRM. Additionally, LRM exhibits physicochemical property issues, such as poor electrical conductivity, slow ion diffusion, and low tap density. In the future, the electrical conductivity, ion diffusion rate, and structural stability of LRM could be improved by constructing a strong network structure of full-surface conductive coating connected with primary particles. Meanwhile, the tap density can be enhanced by filling the internal pores of secondary particles or preparing quasi-monocrystalline LRM.

At the second level, modification strategies have been proposed to address current issues in LRM. However, a single strategy typically addresses part of the problems, and their improvement effects need further enhancement. Therefore, there is an urgent need to refine and integrate existing modification strategies to improve the comprehensive performance of LRM. To enhance the modification strategy, firstly, it is necessary to systematically summarize the process design principles by combining experimental results and theoretical calculation methods. This includes understanding the principle for selecting dopant elements and coating material, as well as lattice matching between coating material and LRM. The second is to improve the accuracy of the modification strategy. This can be achieved through advanced characterization technologies that enable observation and optimization of process conditions, ensuring fixed-point and quantitative doping, coating, and surface interface structure control. Regarding the integration of modification strategies, the modification process can be deeply integrated into the necessary preparation process of LRM, and the integration and comprehensive application of multiple modification strategies can be realized without adding additional process steps and costs. For example, during precursor preparation, morphology and phase composition ratios could be regulated, and dopants could be added. Alternatively, dopants can be introduced during the mixed lithium source stage, followed by simultaneous construction of defects, doping, coating layer, and heterointerface structure during the surface/interface structure optimization process for LRM.

The final level concerns the full lifecycle of LRM, which includes several critical stages that require attention: mass production, packaging and storage, material matching, battery manufacturing, non-destructive testing, failure analysis, cascade utilization, repair activation and recycling. Each key node presents its own set of challenges. Although LRM application in automotive power batteries still requires extensive research, it is possible to select scenarios that prioritize high specific capacity but have lower performance requirements for other aspects. Existing LRM can be applied to manufacturing batteries that are tested and optimized to overcome the critical issues at each node in the full lifecycle of LRM, facilitating their application in more suitable fields. To cater to a broader range of application scenarios, it is essential to continue developing new types of LRM, such as cobalt-free, manganese-rich, high-voltage, solid-state, and wide-temperature-range variants. This ongoing development will help ensure the successful commercialization of LRM.

Author Contributions: Conceptualization, W.G.; writing—original draft preparation, W.G.; writing—review and editing, Z.W., C.Z., M.H., N.S., Q.X. and D.-L.P.; resources, M.H., Q.X. and D.-L.P.; funding acquisition, M.H., Q.X. and D.-L.P.; supervision, M.H., Q.X. and D.-L.P. All authors have read and agreed to the published version of the manuscript.

Funding: The work was supported with financial support from the National Natural Science Foundation of China (Grant Nos. 21671106, 51931006, 52272240, and U22A20118), the Start-Up Fund for High-Levelled Talents from Fujian Normal University, the Fundamental Research Funds for the Central Universities of China (Xiamen University: No. 20720220074), Science and Technology Projects of Innovation Laboratory for Sciences and Technologies of Energy Materials of Fujian Province (H RTP-[2022]-22) and the “Double-First Class” Foundation of Materials Intelligent Manufacturing Discipline of Xiamen University.

Data Availability Statement: Data sharing is not applicable to this article.

Conflicts of Interest: The authors declare no conflict of interest.

References

1. Bielecki, A.; Ernst, S.; Skrodzka, W.; Wojnicki, I. The externalities of energy production in the context of development of clean energy generation. *Environ. Sci. Pollut. Res.* **2020**, *27*, 11506–11530. [[CrossRef](#)] [[PubMed](#)]
2. Lin, B.; Li, Z. Towards world’s low carbon development: The role of clean energy. *Appl. Energy* **2022**, *307*, 118160. [[CrossRef](#)]
3. Lin, J.; Zhang, X.; Fan, E.; Chen, R.; Wu, F.; Li, L. Carbon neutrality strategies for sustainable batteries: From structure, recycling, and properties to applications. *Energy Environ. Sci.* **2023**, *16*, 745–791. [[CrossRef](#)]
4. Ding, Y.; Cano, Z.P.; Yu, A.; Lu, J.; Chen, Z. Automotive Li-ion batteries: Current status and future perspectives. *Electrochem. Energy Rev.* **2019**, *2*, 1–28. [[CrossRef](#)]
5. Zhuo, H.; Peng, H.; Xiao, B.; Wang, Z.; Liu, X.; Li, Z.; Li, G.; Bai, X.; Wang, L.; Huang, X.; et al. Atomic-scale revealing the structure distribution between LiMO_2 and Li_2MnO_3 in Li-rich and Mn-based oxide cathode materials. *Adv. Energy Mater.* **2023**, *13*, 2203354. [[CrossRef](#)]
6. Ellis, B.L.; Lee, K.T.; Nazar, L.F. Positive electrode materials for Li-ion and Li-batteries. *Chem. Mater.* **2010**, *22*, 691–714. [[CrossRef](#)]
7. Malik, R.; Burch, D.; Bazant, M.; Ceder, G. Particle size dependence of the ionic diffusivity. *Nano Lett.* **2010**, *10*, 4123–4127. [[CrossRef](#)]
8. Padhi, A.K.; Nanjundaswamy, K.S.; Goodenough, J.B. Phospho-olivines as positive-electrode materials for rechargeable lithium batteries. *J. Electrochem. Soc.* **1997**, *144*, 1188. [[CrossRef](#)]
9. Yuan, L.-X.; Wang, Z.-H.; Zhang, W.-X.; Hu, X.-L.; Chen, J.-T.; Huang, Y.-H.; Goodenough, J.B. Development and challenges of LiFePO_4 cathode material for lithium-ion batteries. *Energy Environ. Sci.* **2011**, *4*, 269–284. [[CrossRef](#)]
10. Xu, Y.N.; Chung, S.Y.; Bloking, J.T.; Chiang, Y.M.; Ching, W.Y. Electronic structure and electrical conductivity of undoped LiFePO_4 . *Electrochem. Solid-State Lett.* **2004**, *7*, A131–A134. [[CrossRef](#)]
11. Li, L.; Wu, L.; Wu, F.; Song, S.; Zhang, X.; Fu, C.; Yuan, D.; Xiang, Y. Review-recent research progress in surface modification of LiFePO_4 cathode materials. *J. Electrochem. Soc.* **2017**, *164*, A2138. [[CrossRef](#)]
12. Thackeray, M.M. Manganese oxides for lithium batteries. *Prog. Solid State Chem.* **1997**, *25*, 1–71. [[CrossRef](#)]
13. Yang, Y.; Xie, C.; Ruffo, R.; Peng, H.; Kim, D.K.; Cui, Y. Single nanorod devices for battery diagnostics: A case study on LiMn_2O_4 . *Nano Lett.* **2009**, *9*, 4109–4114. [[CrossRef](#)] [[PubMed](#)]
14. Huang, Y.; Dong, Y.; Li, S.; Lee, J.; Wang, C.; Zhu, Z.; Xue, W.; Li, Y.; Li, J. Lithium manganese spinel cathodes for lithium-ion batteries. *Adv. Energy Mater.* **2020**, *11*, 2000997. [[CrossRef](#)]
15. Park, O.K.; Cho, Y.; Lee, S.; Yoo, H.-C.; Song, H.-K.; Cho, J. Who will drive electric vehicles, olivine or spinel? *Energy Environ. Sci.* **2011**, *4*, 1621–1633. [[CrossRef](#)]
16. Thackeray, M.M. Exploiting the spinel structure for Li-ion battery applications: A tribute to John, B. Goodenough. *Adv. Energy Mater.* **2020**, *11*, 2001117–2001124. [[CrossRef](#)]
17. Yang, X.; Sun, X.; Lee, S.J.; McBreen, J.; Mukerjee, S.; Daroux, M.L.; Xing, X.K. In situ synchrotron X-ray diffraction studies of the phase transitions in $\text{Li}_x\text{Mn}_2\text{O}_4$ cathode materials. *Electrochem. Solid-State Lett.* **1999**, *2*, 157–160. [[CrossRef](#)]
18. Zhang, W.; Cupid, D.M.; Gotcu, P.; Chang, K.; Li, D.; Du, Y.; Seifert, H.J. High-throughput description of infinite composition-structure-property-performance relationships of lithium-manganese oxide spinel cathodes. *Chem. Mater.* **2018**, *30*, 2287–2298. [[CrossRef](#)]
19. Gauthier, N.; Courrèges, C.; Demeaux, J.; Tessier, C.; Martinez, H. Impact of the cycling temperature on electrode/electrolyte interfaces within $\text{Li}_4\text{Ti}_5\text{O}_{12}$ vs. LiMn_2O_4 cells. *J. Power Sources* **2020**, *448*, 227573. [[CrossRef](#)]
20. Reimers, J.N.; Dahn, J.R. Electrochemical and in situ X-ray diffraction studies of lithium intercalation in Li_xCoO_2 . *J. Electrochem. Soc.* **1992**, *139*, 2091. [[CrossRef](#)]
21. Zheng, X.; Chen, Y.; Zheng, X.; Zhao, G.; Rui, K.; Li, P.; Xu, X.; Cheng, Z.; Dou, S.X.; Sun, W. Electronic structure engineering of LiCoO_2 toward enhanced oxygen electrocatalysis. *Adv. Energy Mater.* **2019**, *9*, 1803482. [[CrossRef](#)]
22. Manthiram, A. A reflection on lithium-ion battery cathode chemistry. *Nat. Commun.* **2020**, *11*, 1550. [[CrossRef](#)] [[PubMed](#)]

23. Huang, Y.; Zhu, Y.; Fu, H.; Ou, M.; Hu, C.; Yu, S.; Hu, Z.; Chen, C.T.; Jiang, G.; Gu, H.; et al. Mg-pillared LiCoO₂: Towards stable cycling at 4.6 V. *Angew. Chem. Int. Ed.* **2021**, *60*, 4682–4688. [[CrossRef](#)] [[PubMed](#)]
24. Zhu, Z.; Wang, H.; Li, Y.; Gao, R.; Xiao, X.; Yu, Q.; Wang, C.; Waluyo, I.; Ding, J.; Hunt, A.; et al. A surface Se-substituted LiCo[O_{2-δ}Se_δ] cathode with ultrastable high-voltage cycling in pouch full-cells. *Adv. Mater.* **2020**, *32*, 2005182. [[CrossRef](#)] [[PubMed](#)]
25. Li, J.; Lin, C.; Weng, M.; Qiu, Y.; Chen, P.; Yang, K.; Huang, W.; Hong, Y.; Li, J.; Zhang, M.; et al. Structural origin of the high-voltage instability of lithium cobalt oxide. *Nat. Nanotechnol.* **2021**, *16*, 599–605. [[CrossRef](#)]
26. Liu, Q.; Su, X.; Lei, D.; Qin, Y.; Wen, J.; Guo, F.; Wu, Y.A.; Rong, Y.; Kou, R.; Xiao, X.; et al. Approaching the capacity limit of lithium cobalt oxide in lithium ion batteries via lanthanum and aluminium doping. *Nat. Energy* **2018**, *3*, 936–943. [[CrossRef](#)]
27. Lyu, Y.; Wu, X.; Wang, K.; Feng, Z.; Cheng, T.; Liu, Y.; Wang, M.; Chen, R.; Xu, L.; Zhou, J.; et al. An overview on the advances of LiCoO₂ cathodes for lithium-ion batteries. *Adv. Energy Mater.* **2020**, *11*, 2000982. [[CrossRef](#)]
28. Armstrong, A.R.; Bruce, P.G. Synthesis of layered LiMnO₂ as an electrode for rechargeable lithium batteries. *Nature* **1996**, *381*, 499–500. [[CrossRef](#)]
29. Croguennec, L.; Deniard, P.; Brec, R. Electrochemical cyclability of orthorhombic LiMnO₂: Characterization of cycled materials. *J. Electrochem. Soc.* **1997**, *144*, 3323. [[CrossRef](#)]
30. Mishra, S.K.; Ceder, G. Structural stability of lithium manganese oxides. *Phys. Rev. B* **1999**, *59*, 6120. [[CrossRef](#)]
31. Lee, Y.S.; Yoshio, M. Preparation of orthorhombic LiMnO₂ material by quenching. *Electrochem. Solid-State Lett.* **2001**, *4*, A166–A169. [[CrossRef](#)]
32. Cho, J. Stabilization of spinel-like phase transformation of *o*-LiMnO₂ during 55 °C cycling by sol-gel coating of CoO. *Chem. Mater.* **2001**, *13*, 4537–4541. [[CrossRef](#)]
33. Wu, S.-H.; Yu, M.-T. Preparation and characterization of *o*-LiMnO₂ cathode materials. *J. Power Sources* **2007**, *165*, 660–665. [[CrossRef](#)]
34. Zhou, H.; Li, Y.; Zhang, J.; Kang, W.; Yu, D.Y.W. Low-temperature direct synthesis of layered *m*-LiMnO₂ for lithium-ion battery applications. *J. Alloys Compd.* **2016**, *659*, 248–254. [[CrossRef](#)]
35. Huang, Z.-F.; Wang, C.-Z.; Meng, X.; Wang, D.-P.; Chen, G. Effects of Al-doping on the stabilization of monoclinic LiMnO₂. *J. Solid State Chem.* **2006**, *179*, 1602–1609. [[CrossRef](#)]
36. Wu, X.M.; Li, R.X.; Chen, S.; He, Z.Q.; Xu, M.F. Comparative study of Co, Cr and Al-doped LiMnO₂ prepared by ion exchange. *Bull. Mater. Sci.* **2008**, *31*, 109–113. [[CrossRef](#)]
37. Liu, J.; Zou, Z.; Zhang, S.; Zhang, H. Structure, modification, and commercialization of high nickel ternary material (LiNi_{0.8}Co_{0.1}Mn_{0.1}O₂ and LiNi_{0.8}Co_{0.15}Al_{0.05}O₂) for lithium ion batteries. *J. Solid State Electrochem.* **2020**, *25*, 387–410. [[CrossRef](#)]
38. Xia, Y.; Zheng, J.; Wang, C.; Gu, M. Designing principle for Ni-rich cathode materials with high energy density for practical applications. *Nano Energy* **2018**, *49*, 434–452. [[CrossRef](#)]
39. Kang, S.; Choi, D.; Lee, H.; Choi, B.; Kang, Y.M. A mechanistic insight into the oxygen redox of Li-rich layered cathodes and their related electronic/atomic behaviors upon cycling. *Adv. Mater.* **2023**, *35*, e2211965. [[CrossRef](#)]
40. Nayak, P.K.; Erickson, E.M.; Schipper, F.; Penki, T.R.; Munichandraiah, N.; Adelhelm, P.; Sclar, H.; Amalraj, F.; Markovsky, B.; Aurbach, D. Review on challenges and recent advances in the electrochemical performance of high capacity Li- and Mn-rich cathode materials for Li-ion batteries. *Adv. Energy Mater.* **2018**, *8*, 1702397. [[CrossRef](#)]
41. Hua, W.; Wang, S.; Knapp, M.; Leake, S.J.; Senyshyn, A.; Richter, C.; Yavuz, M.; Binder, J.R.; Grey, C.P.; Ehrenberg, H.; et al. Structural insights into the formation and voltage degradation of lithium- and manganese-rich layered oxides. *Nat. Commun.* **2019**, *10*, 5365. [[CrossRef](#)] [[PubMed](#)]
42. Takahashi, I.; Maeda, T.; Kiuchi, H.; Nakanishi, K.; Ohma, A.; Hatano, M.; Fukunaga, T.; Ohta, T.; Matsubara, E. Mechanism of structural change and the trigger of electrochemical degradation of Li-Rich layered oxide cathodes during charge-discharge cycles. *ACS Appl. Energy Mater.* **2019**, *2*, 8118–8124. [[CrossRef](#)]
43. Zheng, H.; Hu, Z.; Liu, P.; Xu, W.; Xie, Q.; He, W.; Luo, Q.; Wang, L.; Gu, D.; Qu, B.; et al. Surface Ni-rich engineering towards highly stable Li_{1.2}Mn_{0.54}Ni_{0.13}Co_{0.13}O₂ cathode materials. *Energy Storage Mater.* **2020**, *25*, 76–85. [[CrossRef](#)]
44. Ding, X.; Luo, D.; Cui, J.; Xie, H.; Ren, Q.; Lin, Z. An ultra-long-life lithium-rich Li_{1.2}Mn_{0.6}Ni_{0.2}O₂ cathode by three-in-one surface modification for lithium-ion batteries. *Angew. Chem. Int. Ed.* **2020**, *59*, 7778–7782. [[CrossRef](#)] [[PubMed](#)]
45. Boivin, E.; Guerrini, N.; House, R.A.; Lozano, J.G.; Jin, L.; Rees, G.J.; Somerville, J.W.; Kuss, C.; Roberts, M.R.; Bruce, P.G. The role of Ni and Co in suppressing O-loss in Li-rich layered cathodes. *Adv. Funct. Mater.* **2020**, *31*, 2003660. [[CrossRef](#)]
46. Yoon, M.; Dong, Y.; Hwang, J.; Sung, J.; Cha, H.; Ahn, K.; Huang, Y.; Kang, S.J.; Li, J.; Cho, J. Reactive boride infusion stabilizes Ni-rich cathodes for lithium-ion batteries. *Nat. Energy* **2021**, *6*, 362–371. [[CrossRef](#)]
47. House, R.A.; Marie, J.-J.; Pérez-Osorio, M.A.; Rees, G.J.; Boivin, E.; Bruce, P.G. The role of O₂ in O-redox cathodes for Li-ion batteries. *Nat. Energy* **2021**, *6*, 781–789. [[CrossRef](#)]
48. Li, Z.; Li, Y.; Zhang, M.; Yin, Z.W.; Yin, L.; Xu, S.; Zuo, C.; Qi, R.; Xue, H.; Hu, J.; et al. Modifying Li@Mn₆ superstructure units by Al substitution to enhance the long-cycle performance of Co-free Li-rich cathode. *Adv. Energy Mater.* **2021**, *11*, 2101962. [[CrossRef](#)]
49. Ahn, J.; Kang, J.; Cho, M.K.; Park, H.; Ko, W.; Lee, Y.; Kim, H.S.; Jung, Y.H.; Jeon, T.Y.; Kim, H.; et al. Selective anionic redox and suppressed structural disordering enabling high-energy and long-life Li-rich layered-oxide cathode. *Adv. Energy Mater.* **2021**, *11*, 2102311. [[CrossRef](#)]

50. Sun, J.; Sheng, C.; Cao, X.; Wang, P.; He, P.; Yang, H.; Chang, Z.; Yue, X.; Zhou, H. Restraining oxygen release and suppressing structure distortion in single-crystal Li-rich layered cathode materials. *Adv. Funct. Mater.* **2021**, *32*, 2110295. [[CrossRef](#)]
51. Zhao, H.; Li, W.; Li, J.; Xu, H.; Zhang, C.; Li, J.; Han, C.; Li, Z.; Chu, M.; Qiu, X. Enhance performances of Co-free Li-rich cathode by eutectic melting salt treatment. *Nano Energy* **2022**, *92*, 106760. [[CrossRef](#)]
52. Hu, E.; Yu, X.; Lin, R.; Bi, X.; Lu, J.; Bak, S.; Nam, K.-W.; Xin, H.L.; Jaye, C.; Fischer, D.A.; et al. Evolution of redox couples in Li- and Mn-rich cathode materials and mitigation of voltage fade by reducing oxygen release. *Nat. Energy* **2018**, *3*, 690–698. [[CrossRef](#)]
53. Xu, J.; Wan, J.; Zhang, W.; Li, Y.; Cheng, F.; Cheng, Z.; Xu, Y.; Sun, S.; Li, Q.; Fang, C.; et al. Regulating the unhybridized O 2p orbitals of high-performance Li-rich Mn-based layered oxide cathode by Gd-doping induced bulk oxygen vacancies. *Adv. Funct. Mater.* **2023**, *33*, 2214613. [[CrossRef](#)]
54. Wei, Y.; Cheng, J.; Li, D.; Li, Y.; Zeng, Z.; Liu, H.; Zhang, H.; Ji, F.; Geng, X.; Lu, J.; et al. A structure self-healing Li-rich cathode achieved by lithium supplement of Li-rich LLZO coating. *Adv. Funct. Mater.* **2023**, *33*, 2214775. [[CrossRef](#)]
55. Zeng, L.; Liang, H.; Qiu, B.; Shi, Z.; Cheng, S.; Shi, K.; Liu, Q.; Liu, Z. Voltage decay of Li-rich layered oxides: Mechanism, modification strategies, and perspectives. *Adv. Funct. Mater.* **2023**, *33*, 2213260. [[CrossRef](#)]
56. Johnston, W.D.; Heikes, R.R. A study of the $\text{Li}_x\text{Mn}_{(1-x)}\text{O}$ system. *J. Am. Chem. Soc.* **1956**, *78*, 3255–3260. [[CrossRef](#)]
57. Thackeray, M.M.; David, W.I.F.; Bruce, P.G.; Goodenough, J.B. Lithium insertion into manganese spinels. *Mater. Res. Bull.* **1983**, *18*, 461–472. [[CrossRef](#)]
58. Ceder, G.; Mishra, S.K. The Stability of orthorhombic and monoclinic-layered LiMnO_2 . *Electrochem. Solid-State Lett.* **1999**, *2*, 550–552. [[CrossRef](#)]
59. Kalyani, P.; Chitra, S.; Mohan, T.; Gopukumar, S. Lithium metal rechargeable cells using Li_2MnO_3 as the positive electrode. *J. Power Sources* **1999**, *80*, 103–106. [[CrossRef](#)]
60. Gummow, R.J.; De Kock, A.; Thackeray, M. Improved capacity retention in rechargeable 4 V lithium/lithium-manganese oxide (spinel) cells. *Solid State Ionics* **1994**, *69*, 59–67. [[CrossRef](#)]
61. Thackeray, M.M.; Johnson, C.S.; Vaughey, J.T.; Li, N.; Hackney, S.A. Advances in manganese-oxide ‘composite’ electrodes for lithium-ion batteries. *J. Mater. Chem.* **2005**, *15*, 2257–2267. [[CrossRef](#)]
62. Capitaine, F.; Gravereau, P.; Delmas, C. A new variety of LiMnO_2 with a layered structure. *Solid State Ionics* **1996**, *89*, 197–202. [[CrossRef](#)]
63. Rossouw, M.H.; Thackeray, M.M. Lithium manganese oxides from Li_2MnO_3 for rechargeable lithium battery applications. *Mat. Res. Bull.* **1991**, *26*, 463–473. [[CrossRef](#)]
64. Whittingham, M.S.; Zavalij, P.Y. Manganese dioxides as cathodes for lithium rechargeable cells: The stability challenge. *Solid State Ionics* **2000**, *131*, 109–115. [[CrossRef](#)]
65. Jang, Y.I.; Huang, B.; Chiang, Y.M.; Sadoway, D.R. Stabilization of LiMnO_2 in the α - NaFeO_2 structure type by LiAlO_2 addition. *Electrochem. Solid-State Lett.* **1998**, *1*, 13. [[CrossRef](#)]
66. Davidson, I.J.; McMillan, R.S.; Slegel, H.; Luan, B.; Kargina, I.; Murray, J.J.; Swainson, I.P. Electrochemistry and structure of $\text{Li}_{2-x}\text{Cr}_y\text{Mn}_{2-y}\text{O}_4$ phases. *J. Power Sources* **1999**, *81*, 406–411. [[CrossRef](#)]
67. Armstrong, A.R.; Robertson, A.D.; Bruce, P.G. Structural transformation on cycling layered $\text{Li}(\text{Mn}_{1-y}\text{Co}_y)\text{O}_2$ cathode materials. *Electrochim. Acta* **1999**, *45*, 285–294. [[CrossRef](#)]
68. Robertson, A.D.; Armstrong, A.R.; Bruce, P.G. Layered $\text{Li}_x\text{Mn}_{1-y}\text{Co}_y\text{O}_2$ intercalation electrodes influence of ion exchange on capacity and structure upon cycling. *Chem. Mater.* **2001**, *13*, 2380–2386. [[CrossRef](#)]
69. Spahr, M.E.; Novák, P.; Schnyder, B.; Haas, O.; Nesper, R. Characterization of layered lithium nickel manganese oxides synthesized by a novel oxidative coprecipitation method and their electrochemical performance as lithium insertion electrode materials. *J. Electrochem. Soc.* **1998**, *145*, 1113. [[CrossRef](#)]
70. Ohzuku, T.; Makimura, Y. Layered lithium insertion material of $\text{LiCo}_{1/3}\text{Ni}_{1/3}\text{Mn}_{1/3}\text{O}_2$ for lithium-ion batteries. *Chem. Lett.* **2001**, *30*, 642–643. [[CrossRef](#)]
71. Johnson, C.S.; Li, N.; Vaughey, J.T.; Hackney, S.A.; Thackeray, M.M. Lithium-manganese oxide electrodes with layered-spinel composite structures $x\text{Li}_2\text{MnO}_3 \cdot (1-x)\text{Li}_{1+y}\text{Mn}_{2-y}\text{O}_4$ ($0 < x < 1$, $0 \leq y \leq 0.33$) for lithium batteries. *Electrochem. Commun.* **2005**, *7*, 528–536.
72. McCalla, E.; Lowartz, C.M.; Brown, C.R.; Dahn, J.R. Formation of layered-layered composites in the Li-Co-Mn oxide pseudoternary system during slow cooling. *Chem. Mater.* **2013**, *25*, 912–918. [[CrossRef](#)]
73. Jarvis, K.A.; Wang, C.-C.; Manthiram, A.; Ferreira, P.J. The role of composition in the atomic structure, oxygen loss, and capacity of layered Li-Mn-Ni oxide cathodes. *J. Mater. Chem. A* **2014**, *2*, 1353–1362. [[CrossRef](#)]
74. He, W.; Guo, W.; Wu, H.; Lin, L.; Liu, Q.; Han, X.; Xie, Q.; Liu, P.; Zheng, H.; Wang, L.; et al. Challenges and recent advances in high capacity Li-rich cathode materials for high energy density lithium-ion batteries. *Adv. Mater.* **2021**, *33*, 2005937. [[CrossRef](#)] [[PubMed](#)]
75. Menon, A.S.; Ulusoy, S.; Ojwang, D.O.; Riekehr, L.; Didier, C.; Peterson, V.K.; Salazar-Alvarez, G.; Svedlindh, P.; Edström, K.; Gomez, C.P.; et al. Synthetic pathway determines the nonequilibrium crystallography of Li- and Mn-rich layered oxide cathode materials. *ACS Appl. Energy Mater.* **2021**, *4*, 1924–1935. [[CrossRef](#)]
76. Lu, Z.; Beaulieu, L.Y.; Donabarger, R.A.; Thomas, C.L.; Dahn, J.R. Synthesis, structure, and electrochemical behavior of $\text{Li}[\text{Ni}_x\text{Li}_{1/3-2x/3}\text{Mn}_{2/3-x/3}\text{O}_2]$. *J. Electrochem. Soc.* **2002**, *149*, A778. [[CrossRef](#)]

77. Lu, Z.; Dahn, J.R. Understanding the anomalous capacity of $\text{Li}/\text{Li}[\text{Ni}_x\text{Li}_{(1/3-2x/3)}\text{Mn}_{(2/3-x/3)}]\text{O}_2$ cells using in situ X-ray diffraction and electrochemical studies. *J. Electrochem. Soc.* **2002**, *149*, A815. [[CrossRef](#)]
78. Ammundsen, B.; Paulsen, J.; Davidson, I.; Liu, R.-S.; Shen, C.-H.; Chen, J.-M.; Jang, L.-Y.; Lee, J.-F. Local structure and first cycle redox mechanism of layered $\text{Li}_{1.2}\text{Cr}_{0.4}\text{Mn}_{0.4}\text{O}_2$ cathode material. *J. Electrochem. Soc.* **2002**, *149*, A431. [[CrossRef](#)]
79. Genevois, C.; Koga, H.; Croguennec, L.; Ménétrier, M.; Delmas, C.; Weill, F. Insight into the atomic structure of cycled Lithium-rich layered oxide $\text{Li}_{1.20}\text{Mn}_{0.54}\text{Co}_{0.13}\text{Ni}_{0.13}\text{O}_2$ using HAADF STEM and electron nanodiffraction. *J. Phys. Chem. C* **2014**, *119*, 75–83. [[CrossRef](#)]
80. Thackeray, M.M.; Kang, S.-H.; Johnson, C.S.; Vaughey, J.T.; Benedek, R.; Hackney, S.A. Li_2MnO_3 -stabilized LiMO_2 (M=Mn, Ni, Co) electrodes for lithium-ion batteries. *J. Mater. Chem.* **2007**, *17*, 3112–3125. [[CrossRef](#)]
81. Lu, Z.; Chen, Z.; Dahn, J.R. Lack of cation clustering in $\text{Li}[\text{Ni}_x\text{Li}_{1/3-2x/3}\text{Mn}_{2/3-x/3}]\text{O}_2$ ($0 < x \leq 1/2$) and $\text{Li}[\text{Cr}_x\text{Li}_{(1-x)/3}\text{Mn}_{(2-2x)/3}]\text{O}_2$ ($0 < x < 1$). *Chem. Mater.* **2003**, *15*, 3214–3220.
82. Jarvis, K.A.; Deng, Z.; Allard, L.F.; Manthiram, A.; Ferreira, P.J. Atomic structure of a lithium-rich layered oxide material for lithium-ion batteries: Evidence of a solid solution. *Chem. Mater.* **2011**, *23*, 3614–3621. [[CrossRef](#)]
83. Koga, H.; Croguennec, L.; Mannesiez, P.; Ménétrier, M.; Weill, F.; Bourgeois, L.; Duttine, M.; Suard, E.; Delmas, C. $\text{Li}_{1.20}\text{Mn}_{0.54}\text{Co}_{0.13}\text{Ni}_{0.13}\text{O}_2$ with different particle sizes as attractive positive electrode materials for lithium-ion batteries: Insights into their structure. *J. Phys. Chem. C* **2012**, *116*, 13497–13506. [[CrossRef](#)]
84. Fujii, H.; Ozawa, K.; Mochiku, T. Electron diffraction and high-resolution electron microscopy studies on layered $\text{Li}_{2-\delta}(\text{Mn}_{1-x}\text{Co}_x)_{1+\delta}\text{O}_3$. *J. Solid State Chem.* **2013**, *203*, 345–352. [[CrossRef](#)]
85. Bareño, J.; Balasubramanian, M.; Kang, S.H.; Wen, J.G.; Lei, C.H.; Pol, S.V.; Petrov, I.; Abraham, D.P. Long-range and local structure in the layered oxide $\text{Li}_{1.2}\text{Co}_{0.4}\text{Mn}_{0.4}\text{O}_2$. *Chem. Mater.* **2011**, *23*, 2039–2050. [[CrossRef](#)]
86. Boulineau, A.; Simonin, L.; Colin, J.-F.; Canévet, E.; Daniel, L.; Patoux, S. Evolutions of $\text{Li}_{1.2}\text{Mn}_{0.6}\text{Ni}_{0.18}\text{Mg}_{0.01}\text{O}_2$ during the initial charge/discharge cycle studied by advanced electron microscopy. *Chem. Mater.* **2012**, *24*, 3558–3566. [[CrossRef](#)]
87. Yu, H.; Ishikawa, R.; So, Y.G.; Shibata, N.; Kudo, T.; Zhou, H.; Ikuhara, Y. Direct atomic-resolution observation of two phases in the $\text{Li}_{1.2}\text{Mn}_{0.567}\text{Ni}_{0.166}\text{Co}_{0.067}\text{O}_2$ cathode material for lithium-ion batteries. *Angew. Chem. Int. Ed.* **2013**, *52*, 5969–5973. [[CrossRef](#)] [[PubMed](#)]
88. Bréger, J.; Jiang, M.; Dupré, N.; Meng, Y.S.; Shao-Horn, Y.; Ceder, G.; Grey, C.P. High-resolution X-ray diffraction, DIFFaX, NMR and first principles study of disorder in the Li_2MnO_3 - $\text{Li}[\text{Ni}_{1/2}\text{Mn}_{1/2}]\text{O}_2$ solid solution. *J. Solid State Chem.* **2005**, *178*, 2575–2585. [[CrossRef](#)]
89. Boulineau, A.; Croguennec, L.; Delmas, C.; Weill, F. Reinvestigation of Li_2MnO_3 structure: Electron diffraction and high resolution TEM. *Chem. Mater.* **2009**, *21*, 4216–4222. [[CrossRef](#)]
90. Weill, F.; Tran, N.; Croguennec, L.; Delmas, C. Cation ordering in the layered $\text{Li}_{1+x}(\text{Ni}_{0.425}\text{Mn}_{0.425}\text{Co}_{0.15})_{1-x}\text{O}_2$ materials ($x = 0$ and 0.12). *J. Power Sources* **2007**, *172*, 893–900. [[CrossRef](#)]
91. Zhao, S.; Yan, K.; Zhang, J.; Sun, B.; Wang, G. Reaction mechanisms of layered lithium-rich cathode materials for high-energy lithium-ion batteries. *Angew. Chem., Int. Ed.* **2021**, *60*, 2208–2220. [[CrossRef](#)] [[PubMed](#)]
92. Sathiyaa, M.; Rousse, G.; Ramesha, K.; Laisa, C.P.; Vezin, H.; Sougrati, M.T.; Doublet, M.L.; Foix, D.; Gonbeau, D.; Walker, W.; et al. Reversible anionic redox chemistry in high-capacity layered-oxide electrodes. *Nat. Mater.* **2013**, *12*, 827–835. [[CrossRef](#)] [[PubMed](#)]
93. Seo, D.H.; Lee, J.; Urban, A.; Malik, R.; Kang, S.; Ceder, G. The structural and chemical origin of the oxygen redox activity in layered and cation-disordered Li-excess cathode materials. *Nat. Chem.* **2016**, *8*, 692–697. [[CrossRef](#)] [[PubMed](#)]
94. Liu, H.; Harris, K.J.; Jiang, M.; Wu, Y.; Goward, G.R.; Botton, G.A. Unraveling the rapid performance decay of layered high-energy cathodes: From nanoscale degradation to drastic bulk evolution. *ACS Nano* **2018**, *12*, 2708–2718. [[CrossRef](#)] [[PubMed](#)]
95. Yan, P.; Nie, A.; Zheng, J.; Zhou, Y.; Lu, D.; Zhang, X.; Xu, R.; Belharouak, I.; Zu, X.; Xiao, J.; et al. Evolution of lattice structure and chemical composition of the surface reconstruction layer in $\text{Li}_{1.2}\text{Ni}_{0.2}\text{Mn}_{0.6}\text{O}_2$ cathode material for lithium ion batteries. *Nano Lett.* **2015**, *15*, 514–522. [[CrossRef](#)] [[PubMed](#)]
96. Gu, M.; Belharouak, I.; Zheng, J.; Wu, H.; Xiao, J.; Genc, A.; Amine, K.; Thevuthasan, S.; Baer, D.R.; Zhang, J.-G.; et al. Formation of the spinel phase in the layered composite cathode used in Li-ion batteries. *ACS Nano* **2013**, *7*, 760–767. [[CrossRef](#)] [[PubMed](#)]
97. Lee, W.; Muhammad, S.; Sergey, C.; Lee, H.; Yoon, J.; Kang, Y.M.; Yoon, W.S. Advances in the cathode materials for lithium rechargeable batteries. *Angew. Chem. Int. Ed.* **2020**, *59*, 2578–2605. [[CrossRef](#)]
98. Lei, Y.; Ni, J.; Hu, Z.; Wang, Z.; Gui, F.; Li, B.; Ming, P.; Zhang, C.; Elias, Y.; Aurbach, D.; et al. Surface modification of Li-rich Mn-based layered oxide cathodes: Challenges, materials, methods, and characterization. *Adv. Energy Mater.* **2020**, *10*, 2002506. [[CrossRef](#)]
99. Gou, X.; Hao, Z.; Hao, Z.; Yang, G.; Yang, Z.; Zhang, X.; Yan, Z.; Zhao, Q.; Chen, J. In situ surface self-reconstruction strategies in Li-rich Mn-based layered cathodes for energy-dense Li-ion batteries. *Adv. Funct. Mater.* **2022**, *32*, 2112088. [[CrossRef](#)]
100. Zhang, M.; Kitchaev, D.A.; Lebens-Higgins, Z.; Vinckeviciute, J.; Zuba, M.; Reeves, P.J.; Grey, C.P.; Whittingham, M.S.; Piper, L.F.J.; Van der Ven, A.; et al. Pushing the limit of 3d transition metal-based layered oxides that use both cation and anion redox for energy storage. *Nat. Rev. Mater.* **2022**, *7*, 522–540. [[CrossRef](#)]
101. Zuo, W.; Luo, M.; Liu, X.; Wu, J.; Liu, H.; Li, J.; Winter, M.; Fu, R.; Yang, W.; Yang, Y. Li-rich cathodes for rechargeable Li-based batteries: Reaction mechanisms and advanced characterization techniques. *Energy Environ. Sci.* **2020**, *13*, 4450–4497. [[CrossRef](#)]

102. House, R.A.; Rees, G.J.; Pérez-Osorio, M.A.; Marie, J.-J.; Boivin, E.; Robertson, A.W.; Nag, A.; Garcia-Fernandez, M.; Zhou, K.-J.; Bruce, P.G. First-cycle voltage hysteresis in Li-rich 3d cathodes associated with molecular O₂ trapped in the bulk. *Nat. Energy* **2020**, *5*, 777–785. [[CrossRef](#)]
103. Liu, T.; Liu, J.; Li, L.; Yu, L.; Diao, J.; Zhou, T.; Li, S.; Dai, A.; Zhao, W.; Xu, S.; et al. Origin of structural degradation in Li-rich layered oxide cathode. *Nature* **2022**, *606*, 305–312. [[CrossRef](#)] [[PubMed](#)]
104. Cui, S.L.; Gao, M.Y.; Li, G.R.; Gao, X.P. Insights into Li-rich Mn-based cathode materials with high capacity: From dimension to lattice to atom. *Adv. Energy Mater.* **2021**, *12*, 2003885. [[CrossRef](#)]
105. Zheng, J.; Shi, W.; Gu, M.; Xiao, J.; Zuo, P.; Wang, C.; Zhang, J.-G. Electrochemical kinetics and performance of layered composite cathode material Li[Li_{0.2}Ni_{0.2}Mn_{0.6}]O₂. *J. Electrochem. Soc.* **2013**, *160*, A2212. [[CrossRef](#)]
106. Zheng, J.; Myeong, S.; Cho, W.; Yan, P.; Xiao, J.; Wang, C.; Cho, J.; Zhang, J.G. Li- and Mn-rich cathode materials: Challenges to commercialization. *Adv. Energy Mater.* **2016**, *7*, 1601284. [[CrossRef](#)]
107. Shin, Y.; Ding, H.; Persson, K.A. Revealing the intrinsic Li mobility in the Li₂MnO₃ lithium-excess material. *Chem. Mater.* **2016**, *28*, 2081–2088. [[CrossRef](#)]
108. Wei, G.Z.; Lu, X.; Ke, F.S.; Huang, L.; Li, J.T.; Wang, Z.X.; Zhou, Z.Y.; Sun, S.G. Crystal habit-tuned nanoplate material of Li[Li_{1/3–2x/3}Ni_xMn_{2/3–x/3}]O₂ for high-rate performance lithium-ion batteries. *Adv. Mater.* **2010**, *22*, 4364–4367. [[CrossRef](#)]
109. Chen, L.; Su, Y.; Chen, S.; Li, N.; Bao, L.; Li, W.; Wang, Z.; Wang, M.; Wu, F. Hierarchical Li_{1.2}Ni_{0.2}Mn_{0.6}O₂ nanoplates with exposed {010} planes as high-performance cathode material for lithium-ion batteries. *Adv. Mater.* **2014**, *26*, 6756–6760. [[CrossRef](#)]
110. Xu, M.; Fei, L.; Zhang, W.; Li, T.; Lu, W.; Zhang, N.; Lai, Y.; Zhang, Z.; Fang, J.; Zhang, K.; et al. Tailoring anisotropic Li-ion transport tunnels on orthogonally arranged Li-rich layered oxide nanoplates toward high-performance Li-ion batteries. *Nano Lett.* **2017**, *17*, 1670–1677. [[CrossRef](#)]
111. Yu, C.; Wang, H.; Guan, X.; Zheng, J.; Li, L. Conductivity and electrochemical performance of cathode xLi₂MnO₃·(1–x)LiMn_{1/3}Ni_{1/3}Co_{1/3}O₂ (x = 0.1, 0.2, 0.3, 0.4) at different temperatures. *J. Alloys Compd.* **2013**, *546*, 239–245. [[CrossRef](#)]
112. Chen, H.; Islam, M.S. Lithium extraction mechanism in Li-rich Li₂MnO₃ involving oxygen hole formation and dimerization. *Chem. Mater.* **2016**, *28*, 6656–6663. [[CrossRef](#)]
113. Zheng, J.; Xu, P.; Gu, M.; Xiao, J.; Browning, N.D.; Yan, P.; Wang, C.; Zhang, J.-G. Structural and chemical evolution of Li- and Mn-rich layered cathode material. *Chem. Mater.* **2015**, *27*, 1381–1390. [[CrossRef](#)]
114. Hong, J.; Lim, H.-D.; Lee, M.; Kim, S.-W.; Kim, H.; Oh, S.-T.; Chung, G.-C.; Kang, K. Critical role of oxygen evolved from layered Li-excess metal oxides in lithium rechargeable batteries. *Chem. Mater.* **2012**, *24*, 2692–2697. [[CrossRef](#)]
115. Yan, P.; Zheng, J.; Tang, Z.K.; Devaraj, A.; Chen, G.; Amine, K.; Zhang, J.G.; Liu, L.M.; Wang, C. Injection of oxygen vacancies in the bulk lattice of layered cathodes. *Nat. Nanotechnol.* **2019**, *14*, 602–608. [[CrossRef](#)] [[PubMed](#)]
116. Li, Q.; Ning, D.; Wong, D.; An, K.; Tang, Y.; Zhou, D.; Schuck, G.; Chen, Z.; Zhang, N.; Liu, X. Improving the oxygen redox reversibility of Li-rich battery cathode materials via Coulombic repulsive interactions strategy. *Nat. Commun.* **2022**, *13*, 1123. [[CrossRef](#)] [[PubMed](#)]
117. Kawai, K.; Sudayama, T.; Asakura, D.; Kikkawa, J.; Watanabe, E.; Okubo, M.; Yamada, A. High-voltage electrochemical properties of lithium-rich spinel oxides. *J. Phys. Chem. C* **2023**, *127*, 12428–12434. [[CrossRef](#)]
118. Pan, H.; Jiao, S.; Xue, Z.; Zhang, J.; Xu, X.; Gan, L.; Li, Q.; Liu, Y.; Yu, X.; Li, H.; et al. The roles of Ni and Mn in the thermal stability of lithium-rich manganese-rich oxide cathode. *Adv. Energy Mater.* **2023**, *13*, 2203989. [[CrossRef](#)]
119. Wang, G.; Wang, X.; Yi, L.; Yu, R.; Liu, M.; Yang, X. Preparation and performance of 0.5Li₂MnO₃·0.5LiNi_{1/3}Co_{1/3}Mn_{1/3}O₂ with a fusiform porous micro-nano structure. *J. Mater. Chem. A* **2016**, *4*, 15929–15939. [[CrossRef](#)]
120. Ma, Y.; Liu, P.; Xie, Q.; Zhang, G.; Zheng, H.; Cai, Y.; Li, Z.; Wang, L.; Zhu, Z.Z.; Mai, L.; et al. Double-shell Li-rich layered oxide hollow microspheres with sandwich-like carbon@spinel@layered@spinel@carbon shells as high-rate lithium ion battery cathode. *Nano Energy* **2019**, *59*, 184–196. [[CrossRef](#)]
121. Deng, B.; Chen, Y.; Wu, P.; Han, J.; Li, Y.; Zheng, H.; Xie, Q.; Wang, L.; Peng, D.-L. Lithium-rich layered oxide nanowires bearing porous structures and spinel domains as cathode materials for lithium-ion batteries. *J. Power Sources* **2019**, *418*, 122–129. [[CrossRef](#)]
122. Liu, Q.; Xie, T.; Xie, Q.; He, W.; Zhang, Y.; Zheng, H.; Lu, X.; Wei, W.; Sa, B.; Wang, L.; et al. Multiscale deficiency integration by Na-rich engineering for high-stability Li-rich layered oxide cathodes. *ACS Appl. Mater. Interfaces* **2021**, *13*, 8239–8248. [[CrossRef](#)] [[PubMed](#)]
123. Liu, Y.; Wang, J.; Wu, J.; Ding, Z.; Yao, P.; Zhang, S.; Chen, Y. 3D cube-maze-like Li-rich layered cathodes assembled from 2D porous nanosheets for enhanced cycle stability and rate capability of lithium-ion batteries. *Adv. Energy Mater.* **2019**, *10*, 1903139. [[CrossRef](#)]
124. Wu, T.; Liu, X.; Zhang, X.; Lu, Y.; Wang, B.; Deng, Q.; Yang, Y.; Wang, E.; Lyu, Z.; Li, Y.; et al. Full concentration gradient-tailored Li-rich layered oxides for high-energy lithium-ion batteries. *Adv. Mater.* **2021**, *33*, 2001358. [[CrossRef](#)]
125. Zuo, Y.; Li, B.; Jiang, N.; Chu, W.; Zhang, H.; Zou, R.; Xia, D. A high-capacity O₂-type Li-rich cathode material with a single-layer Li₂MnO₃ superstructure. *Adv. Mater.* **2018**, *30*, 1707255. [[CrossRef](#)] [[PubMed](#)]
126. de Boisse, B.M.; Jang, J.; Okubo, M.; Yamada, A. Cobalt-free O₂-type lithium-rich layered oxides. *J. Electrochem. Soc.* **2018**, *165*, A3630. [[CrossRef](#)]
127. Shang, H.; Zuo, Y.; Shen, F.; Song, J.; Ning, F.; Zhang, K.; He, L.; Xia, D. O₂-type Li_{0.78}[Li_{0.24}Mn_{0.76}]O₂ nanowires for high-performance lithium-ion battery cathode. *Nano Lett.* **2020**, *20*, 5779–5785. [[CrossRef](#)] [[PubMed](#)]

128. Eum, D.; Kim, B.; Kim, S.J.; Park, H.; Wu, J.; Cho, S.P.; Yoon, G.; Lee, M.H.; Jung, S.K.; Yang, W.; et al. Voltage decay and redox asymmetry mitigation by reversible cation migration in lithium-rich layered oxide electrodes. *Nat. Mater.* **2020**, *19*, 419–427. [[CrossRef](#)]
129. Wu, F.; Li, N.; Su, Y.; Shou, H.; Bao, L.; Yang, W.; Zhang, L.; An, R.; Chen, S. Spinel/layered heterostructured cathode material for high-capacity and high-rate Li-ion batteries. *Adv. Mater.* **2013**, *25*, 3722–3726. [[CrossRef](#)]
130. Zhao, J.; Huang, R.; Gao, W.; Zuo, J.-M.; Zhang, X.F.; Mixture, S.T.; Chen, Y.; Lockard, J.V.; Zhang, B.; Guo, S.; et al. An ion-exchange promoted phase transition in a Li-excess layered cathode material for high-performance lithium ion batteries. *Adv. Energy Mater.* **2015**, *5*, 1401937–1401948. [[CrossRef](#)]
131. Deng, Y.-P.; Fu, F.; Wu, Z.-G.; Yin, Z.-W.; Zhang, T.; Li, J.-T.; Huang, L.; Sun, S.-G. Layered/spinel heterostructured Li-rich materials synthesized by a one-step solvothermal strategy with enhanced electrochemical performance for Li-ion batteries. *J. Mater. Chem. A* **2016**, *4*, 257–263. [[CrossRef](#)]
132. Zhang, X.D.; Shi, J.L.; Liang, J.Y.; Yin, Y.X.; Zhang, J.N.; Yu, X.Q.; Guo, Y.G. Suppressing surface lattice oxygen release of Li-rich cathode materials via heterostructured spinel $\text{Li}_4\text{Mn}_5\text{O}_{12}$ coating. *Adv. Mater.* **2018**, *30*, 1801751. [[CrossRef](#)] [[PubMed](#)]
133. Kim, S.; Cho, W.; Zhang, X.; Oshima, Y.; Choi, J.W. A stable lithium-rich surface structure for lithium-rich layered cathode materials. *Nat. Commun.* **2016**, *7*, 13598. [[CrossRef](#)] [[PubMed](#)]
134. Yang, S.; Wang, P.; Wei, H.; Tang, L.; Zhang, X.; He, Z.; Li, Y.; Tong, H.; Zheng, J. $\text{Li}_4\text{V}_2\text{Mn}(\text{PO}_4)_4$ -stabilized $\text{Li}[\text{Li}_{0.2}\text{Mn}_{0.54}\text{Ni}_{0.13}\text{Co}_{0.13}]\text{O}_2$ cathode materials for lithium ion batteries. *Nano Energy* **2019**, *63*, 103889. [[CrossRef](#)]
135. Zheng, F.; Yang, C.; Xiong, X.; Xiong, J.; Hu, R.; Chen, Y.; Liu, M. Nanoscale surface modification of lithium-rich layered-oxide composite cathodes for suppressing voltage fade. *Angew. Chem. Int. Ed.* **2015**, *54*, 13058–13062. [[CrossRef](#)] [[PubMed](#)]
136. Zhang, X.; Belharouak, I.; Li, L.; Lei, Y.; Elam, J.W.; Nie, A.; Chen, X.; Yassar, R.S.; Axelbaum, R.L. Structural and electrochemical study of Al_2O_3 and TiO_2 coated $\text{Li}_{1.2}\text{Ni}_{0.13}\text{Mn}_{0.54}\text{Co}_{0.13}\text{O}_2$ cathode material using ALD. *Adv. Energy Mater.* **2013**, *3*, 1299–1307. [[CrossRef](#)]
137. Zhou, Z.; Luo, Z.; He, Z.; Zheng, J.; Li, Y.; Yan, C.; Mao, J. Suppress voltage decay of lithium-rich materials by coating layers with different crystalline states. *J. Energy Chem.* **2021**, *60*, 591–598. [[CrossRef](#)]
138. Wang, Z.; Liu, E.; He, C.; Shi, C.; Li, J.; Zhao, N. Effect of amorphous FePO_4 coating on structure and electrochemical performance of $\text{Li}_{1.2}\text{Ni}_{0.13}\text{Co}_{0.13}\text{Mn}_{0.54}\text{O}_2$ as cathode material for Li-ion batteries. *J. Power Sources* **2013**, *236*, 25–32. [[CrossRef](#)]
139. Xiao, B.; Wang, B.; Liu, J.; Kaliyappan, K.; Sun, Q.; Liu, Y.; Dadheech, G.; Balogh, M.P.; Yang, L.; Sham, T.-K.; et al. Highly stable $\text{Li}_{1.2}\text{Mn}_{0.54}\text{Co}_{0.13}\text{Ni}_{0.13}\text{O}_2$ enabled by novel atomic layer deposited AlPO_4 coating. *Nano Energy* **2017**, *34*, 120–130. [[CrossRef](#)]
140. Sun, Y.K.; Lee, M.J.; Yoon, C.S.; Hassoun, J.; Amine, K.; Scrosati, B. The role of AlF_3 coatings in improving electrochemical cycling of Li-enriched nickel-manganese oxide electrodes for Li-ion batteries. *Adv. Mater.* **2012**, *24*, 1192–1196. [[CrossRef](#)]
141. Chong, S.; Chen, Y.; Yan, W.; Guo, S.; Tan, Q.; Wu, Y.; Jiang, T.; Liu, Y. Suppressing capacity fading and voltage decay of Li-rich layered cathode material by a surface nano-protective layer of CoF_2 for lithium-ion batteries. *J. Power Sources* **2016**, *332*, 230–239. [[CrossRef](#)]
142. Martha, S.K.; Nanda, J.; Kim, Y.; Unocic, R.R.; Pannala, S.; Dudney, N.J. Solid electrolyte coated high voltage layered-layered lithium-rich composite cathode: $\text{Li}_{1.2}\text{Mn}_{0.525}\text{Ni}_{0.175}\text{Co}_{0.1}\text{O}_2$. *J. Mater. Chem. A* **2013**, *1*, 5587–5595. [[CrossRef](#)]
143. Fu, Q.; Du, F.; Bian, X.; Wang, Y.; Yan, X.; Zhang, Y.; Zhu, K.; Chen, G.; Wang, C.; Wei, Y. Electrochemical performance and thermal stability of $\text{Li}_{1.18}\text{Co}_{0.15}\text{Ni}_{0.15}\text{Mn}_{0.52}\text{O}_2$ surface coated with the ionic conductor Li_3VO_4 . *J. Mater. Chem. A* **2014**, *2*, 7555–7562. [[CrossRef](#)]
144. Xu, Z.; Ci, L.; Yuan, Y.; Nie, X.; Li, J.; Cheng, J.; Sun, Q.; Zhang, Y.; Han, G.; Min, G.; et al. Potassium prussian blue-coated Li-rich cathode with enhanced lithium ion storage property. *Nano Energy* **2020**, *75*, 104942. [[CrossRef](#)]
145. Si, M.; Wang, D.; Zhao, R.; Pan, D.; Zhang, C.; Yu, C.; Lu, X.; Zhao, H.; Bai, Y. Local electric-field-driven fast Li diffusion kinetics at the piezoelectric LiTaO_3 modified Li-rich cathode-electrolyte interphase. *Adv. Sci.* **2020**, *7*, 1902538. [[CrossRef](#)]
146. Zhang, W.; Sun, Y.; Deng, H.; Ma, J.; Zeng, Y.; Zhu, Z.; Lv, Z.; Xia, H.; Ge, X.; Cao, S.; et al. Dielectric polarization in inverse spinel-structured Mg_2TiO_4 coating to suppress oxygen evolution of Li-rich cathode materials. *Adv. Mater.* **2020**, *32*, 2000496. [[CrossRef](#)] [[PubMed](#)]
147. Qing, R.-P.; Shi, J.-L.; Xiao, D.-D.; Zhang, X.-D.; Yin, Y.-X.; Zhai, Y.-B.; Gu, L.; Guo, Y.-G. Enhancing the kinetics of Li-rich cathode materials through the pinning effects of gradient surface Na^+ doping. *Adv. Energy Mater.* **2016**, *6*, 1501914. [[CrossRef](#)]
148. He, W.; Liu, P.; Qu, B.; Zheng, Z.; Zheng, H.; Deng, P.; Li, P.; Li, S.; Huang, H.; Wang, L.; et al. Uniform Na^+ doping-induced defects in Li- and Mn-rich cathodes for high-performance lithium-ion batteries. *Adv. Sci.* **2019**, *6*, 1802114–1802124. [[CrossRef](#)]
149. Wang, Q.; He, W.; Wang, L.; Li, S.; Zheng, H.; Liu, Q.; Cai, Y.; Lin, J.; Xie, Q.; Peng, D.-L. Morphology control and Na^+ doping toward high-performance Li-rich layered cathode materials for lithium-ion batteries. *ACS Sustain. Chem. Eng.* **2020**, *9*, 197–206. [[CrossRef](#)]
150. Ding, X.; Li, Y.X.; He, X.D.; Liao, J.Y.; Hu, Q.; Chen, F.; Zhang, X.Q.; Zhao, Y.; Chen, C.H. Surface Li^+/K^+ exchange toward double-gradient modification of layered Li-rich cathode materials. *ACS Appl. Mater. Interfaces* **2019**, *11*, 31477–31483. [[CrossRef](#)]
151. Choi, A.; Lim, J.; Kim, H.-J.; Jung, S.C.; Lim, H.-W.; Kim, H.; Kwon, M.-S.; Han, Y.K.; Oh, S.M.; Lee, K.T. Site-selective in situ electrochemical doping for Mn-rich layered oxide cathode materials in lithium-ion batteries. *Adv. Energy Mater.* **2018**, *8*, 1702514. [[CrossRef](#)]
152. Li, Y.; Xu, S.; Zhao, W.; Chen, Z.; Chen, Z.; Li, S.; Hu, J.; Cao, B.; Li, J.; Zheng, S.; et al. Correlating the dispersion of $\text{Li}@\text{Mn}_6$ superstructure units with the oxygen activation in Li-rich layered cathode. *Energy Storage Mater.* **2022**, *45*, 422–431. [[CrossRef](#)]

153. Liu, S.; Liu, Z.; Shen, X.; Li, W.; Gao, Y.; Banis, M.N.; Li, M.; Chen, K.; Zhu, L.; Yu, R.; et al. Surface doping to enhance structural integrity and performance of Li-rich layered oxide. *Adv. Energy Mater.* **2018**, *8*, 1802105. [[CrossRef](#)]
154. Huang, J.; Liu, H.; Hu, T.; Meng, Y.S.; Luo, J. Enhancing the electrochemical performance of Li-rich layered oxide $\text{Li}_{1.13}\text{Ni}_{0.3}\text{Mn}_{0.57}\text{O}_2$ via WO_3 doping and accompanying spontaneous surface phase formation. *J. Power Sources* **2018**, *375*, 21–28. [[CrossRef](#)]
155. Meng, J.; Xu, L.; Ma, Q.; Yang, M.; Fang, Y.; Wan, G.; Li, R.; Yuan, J.; Zhang, X.; Yu, H.; et al. Modulating crystal and interfacial properties by W-gradient doping for highly stable and long life Li-rich layered cathodes. *Adv. Funct. Mater.* **2022**, *32*, 2113013. [[CrossRef](#)]
156. Chen, S.; Xie, Y.; Chen, W.; Chen, J.; Yang, W.; Zou, H.; Lin, Z. Enhanced electrochemical performance of Li-rich cathode materials by organic fluorine doping and spinel $\text{Li}_{1+x}\text{Ni}_y\text{Mn}_{2-y}\text{O}_4$ coating. *ACS Sustain. Chem. Eng.* **2019**, *8*, 121–128. [[CrossRef](#)]
157. Pei, Y.; Li, S.; Chen, Q.; Liang, R.; Li, M.; Gao, R.; Ren, D.; Deng, Y.-P.; Jin, H.; Wang, S.; et al. Cationic-anionic redox couple gradient to immunize against irreversible processes of Li-rich layered oxides. *J. Mater. Chem. A* **2021**, *9*, 2325–2333. [[CrossRef](#)]
158. Zhang, K.; Qi, J.; Song, J.; Zuo, Y.; Yang, Y.; Yang, T.; Chen, T.; Liu, X.; Chen, L.; Xia, D. Sulfuration of Li-rich Mn-based cathode materials for multianionic redox and stabilized coordination environment. *Adv. Mater.* **2022**, *34*, 2109564. [[CrossRef](#)]
159. Li, B.; Yan, H.; Ma, J.; Yu, P.; Xia, D.; Huang, W.; Chu, W.; Wu, Z. Manipulating the electronic structure of Li-rich manganese-based oxide using polyanions: Towards better electrochemical performance. *Adv. Funct. Mater.* **2014**, *24*, 5112–5118. [[CrossRef](#)]
160. Li, Q.; Ning, D.; Zhou, D.; An, K.; Schuck, G.; Wong, D.; Kong, W.; Schulz, C.; Schumacher, G.; Liu, X. Tuning both anionic and cationic redox chemistry of Li-rich $\text{Li}_{1.2}\text{Mn}_{0.6}\text{Ni}_{0.2}\text{O}_2$ via a “three-in-one” strategy. *Chem. Mater.* **2020**, *32*, 9404–9414. [[CrossRef](#)]
161. Wang, E.; Xiao, D.; Wu, T.; Liu, X.; Zhou, Y.; Wang, B.; Lin, T.; Zhang, X.; Yu, H. Al/Ti synergistic doping enhanced cycle stability of Li-rich layered oxides. *Adv. Funct. Mater.* **2022**, *32*, 2201744. [[CrossRef](#)]
162. Yu, Y.; Yang, Z.; Zhong, J.; Liu, Y.; Li, J.; Wang, X.; Kang, F. A simple dual-ion doping method for stabilizing Li-rich materials and suppressing voltage decay. *ACS Appl. Mater. Interfaces* **2020**, *12*, 13996–14004. [[CrossRef](#)]
163. Nie, L.; Wang, Z.; Zhao, X.; Chen, S.; He, Y.; Zhao, H.; Gao, T.; Zhang, Y.; Dong, L.; Kim, F.; et al. Cation/anion codoped and cobalt-free Li-rich layered cathode for high-performance Li-ion batteries. *Nano Lett.* **2021**, *21*, 8370–8377. [[CrossRef](#)]
164. Lee, J.; Kitchaev, D.A.; Kwon, D.H.; Lee, C.W.; Papp, J.K.; Liu, Y.S.; Lun, Z.; Clement, R.J.; Shi, T.; McCloskey, B.D.; et al. Reversible $\text{Mn}^{2+}/\text{Mn}^{4+}$ double redox in lithium-excess cathode materials. *Nature* **2018**, *556*, 185–190. [[CrossRef](#)]
165. Ding, X.; Li, Y.-X.; Wang, S.; Dong, J.-M.; Yasmin, A.; Hu, Q.; Wen, Z.-Y.; Chen, C.-H. Towards improved structural stability and electrochemical properties of a Li-rich material by a strategy of double gradient surface modification. *Nano Energy* **2019**, *61*, 411–419. [[CrossRef](#)]
166. Zheng, H.; Zhang, C.; Zhang, Y.; Lin, L.; Liu, P.; Wang, L.; Wei, Q.; Lin, J.; Sa, B.; Xie, Q.; et al. Manipulating the local electronic structure in Li-rich layered cathode towards superior electrochemical performance. *Adv. Funct. Mater.* **2021**, *31*, 2100783–2100795. [[CrossRef](#)]
167. Liu, P.; Zhang, H.; He, W.; Xiong, T.; Cheng, Y.; Xie, Q.; Ma, Y.; Zheng, H.; Wang, L.; Zhu, Z.Z.; et al. Lithium deficiencies engineering in Li-rich layered oxide $\text{Li}_{1.098}\text{Mn}_{0.533}\text{Ni}_{0.113}\text{Co}_{0.138}\text{O}_2$ for high-stability cathode. *J. Am. Chem. Soc.* **2019**, *141*, 10876–10882. [[CrossRef](#)]
168. Li, S.; Zhang, H.; Li, H.; Zhang, S.; Zhu, B.; Wang, S.; Zheng, J.; Liu, F.; Zhang, Z.; Lai, Y. Enhanced activity and reversibility of anionic redox by tuning lithium vacancies in Li-rich cathode materials. *ACS Appl. Mater. Interfaces* **2021**, *13*, 39480–39490. [[CrossRef](#)]
169. Qiu, B.; Zhang, M.; Wu, L.; Wang, J.; Xia, Y.; Qian, D.; Liu, H.; Hy, S.; Chen, Y.; An, K.; et al. Gas-solid interfacial modification of oxygen activity in layered oxide cathodes for lithium-ion batteries. *Nat. Commun.* **2016**, *7*, 12108. [[CrossRef](#)]
170. Sun, Y.; Cong, H.; Zan, L.; Zhang, Y. Oxygen vacancies and stacking faults introduced by low-temperature reduction improve the electrochemical properties of Li_2MnO_3 nanobelts as lithium-ion battery cathodes. *ACS Appl. Mater. Interfaces* **2017**, *9*, 38545–38555. [[CrossRef](#)]
171. Cui, S.L.; Zhang, X.; Wu, X.W.; Liu, S.; Zhou, Z.; Li, G.R.; Gao, X.P. Understanding the structure-performance relationship of lithium-rich cathode materials from an oxygen-vacancy perspective. *ACS Appl. Mater. Interfaces* **2020**, *12*, 47655–47666. [[CrossRef](#)]
172. Liu, J.; Hou, M.; Yi, J.; Guo, S.; Wang, C.; Xia, Y. Improving the electrochemical performance of layered lithium-rich transition-metal oxides by controlling the structural defects. *Energy Environ. Sci.* **2014**, *7*, 705–714. [[CrossRef](#)]
173. Guo, H.; Wei, Z.; Jia, K.; Qiu, B.; Yin, C.; Meng, F.; Zhang, Q.; Gu, L.; Han, S.; Liu, Y.; et al. Abundant nanoscale defects to eliminate voltage decay in Li-rich cathode materials. *Energy Storage Mater.* **2019**, *16*, 220–227. [[CrossRef](#)]
174. Yang, J.; Li, P.; Zhong, F.; Feng, X.; Chen, W.; Ai, X.; Yang, H.; Xia, D.; Cao, Y. Suppressing voltage fading of Li-rich oxide cathode via building a well-protected and partially-protonated surface by polyacrylic acid binder for cycle-stable Li-ion batteries. *Adv. Energy Mater.* **2020**, *10*, 1904264. [[CrossRef](#)]
175. Xu, Z.; Guo, X.; Wang, J.; Yuan, Y.; Sun, Q.; Tian, R.; Yang, H.; Lu, J. Restraining the octahedron collapse in lithium and manganese rich NCM cathode toward suppressing structure transformation. *Adv. Energy Mater.* **2022**, *12*, 2201323. [[CrossRef](#)]

Disclaimer/Publisher’s Note: The statements, opinions and data contained in all publications are solely those of the individual author(s) and contributor(s) and not of MDPI and/or the editor(s). MDPI and/or the editor(s) disclaim responsibility for any injury to people or property resulting from any ideas, methods, instructions or products referred to in the content.